Palaeogeography, Palaeoclimatology, Palaeoecology 696 (2026) 113874

Contents lists available at ScienceDirect

Palaeogeography, Palaeoclimatology, Palaeoecology

journal homepage: www.elsevier.com/locate/palaeo

Mesophotic normality: Lower Miocene coral bioherms pioneering the incipient Red Sea

Guillem Mateu-Vicens [a], Marco Brandano [b], Patrick Boyden [c], Andrea Benedetti [d], Jan-Peter Duda [e], Hildegard Westphal [f,g,h,*]

[a] Department of Biology, Universitat de les Illes Balears, Spain
[b] Dipartimento di Scienze della Terra, La Sapienza Università di Roma, Italy
[c] MARUM Center for Marine Environmental Sciences, University of Bremen, Bremen, Germany
[d] Dipartimento di Scienze Naturali, Liceo Isabella d'Este, Tivoli, Italy
[e] Department of Geobiology, Geoscience Center, University of Göttingen, Germany
[f] Leibniz Centre for Tropical Marine Research (ZMT), Germany
[g] Department of Geosciences, University of Bremen, Germany
[h] Division of Physical Sciences and Engineering (PSE), King Abdullah University of Science and Technology (KAUST), Saudi Arabia

ARTICLE INFO

Editor: M. Elliot

Keywords:
Coral bioherms
Coral mounds
Burdigalian
Red Sea
Palecology
Stratigraphy
Mesophotic

ABSTRACT

The southernmost Miocene coral bioherms in western Saudi Arabia (Wadi Waqb Member) record a short episode of coral growth in the incipient Red Sea that was terminated by a salinity crisis. Here, we investigate the paleoecological significance of these coral-dominated deposits to better understand ecosystem dynamics during the early stages of Red Sea basin evolution. The coral bioherms form mound stacks on a ramp-like slope morphology predefined by an unconformity on the underlying Precambrian to Cenozoic basement complex. Thus, they are distinctly different from modern tropical coral reefs with their typical geometry of shallow fringing reef and back-reef lagoons. The Miocene bioherms are embedded in fine-grained sediment containing planktonic foraminifera, suggesting an open marine setting below storm wave base, consistent with meso- to oligophotic conditions. Euphotic allochems such as *Halimeda* plates and benthic foraminifera (including abundant epiphytic taxa) are interpreted to have been shed downslope from shallow water areas such as seagrass meadows. Notably, the large benthic foraminifer *Miogypsina globulina* is recorded for the first time in Saudi Arabia, allowing us to assign the lower investigated succession to the Burdigalian and to identify the Burdigalian–Langhian transition, thus refining the previous age determination of the Wadi Waqb Member based on planktonic foraminifera. The precise age enables correlation of the investigated deposits in a context with upper Oligocene to Lower/Middle Miocene successions in the Mediterranean, revealing strong paleoenvironmental similarities, including the dominance of massive coral growth, similar to modern meso-oligophotic settings. As the Wadi Waqb Member was deposited before the global cooling trend of the Middle to Late Miocene, our findings support the notion that the ecology of early Cenozoic coral ecosystems was fundamentally different from modern corals reefs that migrated upward in the water column into shallower water environments during the Tortonian.

1. Introduction

The early development of coral bioconstructions in the Red Sea represents a key—but still poorly understood—episode within the Miocene ecological reorganization of tropical shallow-marine ecosystems. During the Early to Middle Miocene, the Red Sea formed as an incipient ocean basin resulting from the fragmentation of the Tethyan realm, and occupied a cul-de-sac paleogeographic position of the Mediterranean that likely imposed particular oceanographic, hydrochemical, and biogeographic constraints on reef-building organisms (Perrin, 2002; Bosworth et al., 2005; Torfstein and Steinberg, 2020; Pisapia et al., 2024). Despite several studies describing Miocene coral occurrences along the Red Sea margins (Egypt: Perrin et al., 1998; the Midyan area, i.e., the Northern Red Sea coast of Saudi Arabia: Hughes

* Corresponding author at: Leibniz Centre for Tropical Marine Research (ZMT), Germany.
E-mail address: hildegard.westphal@leibniz-zmt.de (H. Westphal).

https://doi.org/10.1016/j.palaeo.2026.113874
Received 30 April 2025; Received in revised form 26 February 2026; Accepted 5 May 2026
Available online 8 May 2026

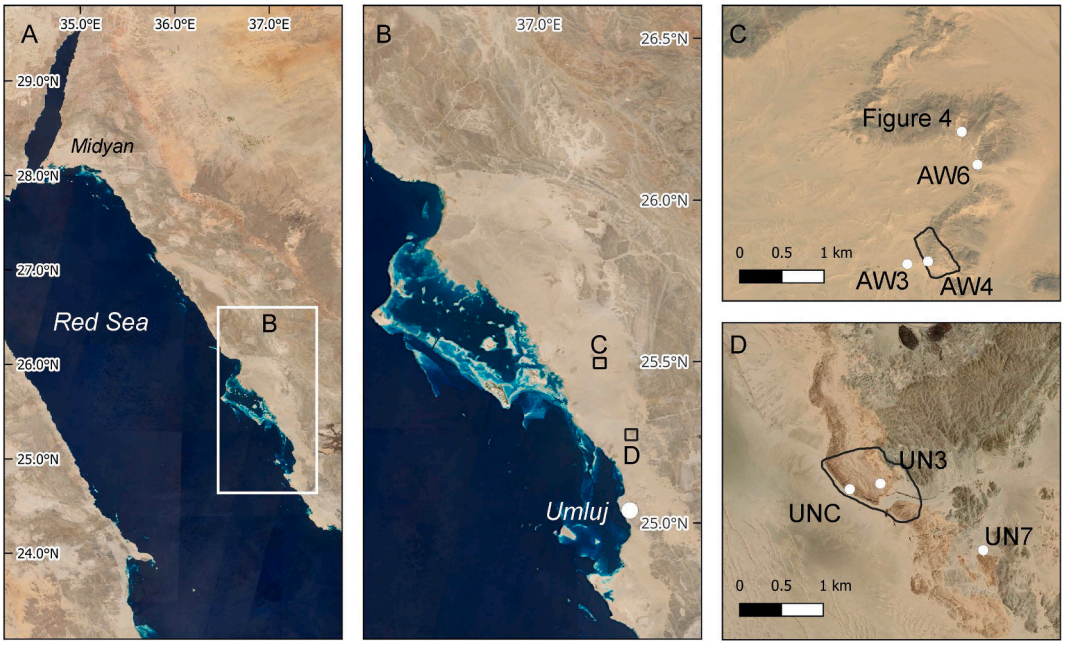

Fig. 1. (A) Location of the study area in the northern Red Sea; (B) Study area to the north of the town of Umluj; (C) close-up of the Al-Wajh site with outline of the orthomosaic and locations of the Al-Wajh sections (AW3, AW4, AW6) and location of Fig. 4 indicated; (D) close-up of the Umluj site with outline of the orthomosaic and locations of the Umluj sections (UNC, UN3, UN7) indicated. Satellite imagery from Sentinel-2, Copernicus Sentinel data [2024]. (For interpretation of the references to colour in this figure legend, the reader is referred to the web version of this article.)

and Johnson, 2005; Hughes, 2014; El-Sorogy et al., 2020; in the study area: Pisapia et al., 2024), these deposits have neither been evaluated within the framework of the major Cenozoic shift from larger benthic foraminifera (LBF)-dominated carbonate systems to coral-coralline algal ecosystems (Pomar et al., 2017), nor in terms of the ecological drivers that enabled the first establishment of coral bioherms in this restricted basin.

During the Cenozoic, tropical to subtropical shallow-marine carbonate systems underwent a profound ecological transformation associated with significant changes in the biota and resulting in differences in depositional architecture (Pomar, 2020). Paleogene platforms were largely dominated by non-framework building biota, particularly photosymbiotic LBF such as nummulitids, discocyclinids, alveolinids, and orthophragmines, together with molluscs and echinoderms. These assemblages thrived under warm, meso-oligotrophic conditions, with a weakly stratified water column limiting vertical nutrient flux. During the Eocene-Oligocene transition, associated with a major cooling step, the carbonate factory underwent a significant shift with the spreading of coral bioconstructions (Pomar et al., 2017). More specifically, carbonate ramps with coral mounds are documented in the Rupelian of the Castelgomberto Limestone unit (Lessini Mountains, Southern Alps of Northern Italy: Tusberti et al., 2024) and the Majella (Central Apennines, Italy: Vecsei and Sanders, 1997; Brandano et al., 2019), as well as in the Chattian of the Salento (southern Italy: Pomar et al., 2014; Bosellini et al., 2021). The subsequent progressive ecological expansion of scleractinian coral bioconstructions from meso-oligophotic into euphotic settings during the Middle to Late Miocene marks a sharp transition in which framework-building organisms became increasingly important carbonate producers (Montaggioni and Braithwaite, 2009; Pomar et al., 2017).

The marked biotic shift from LBF-dominated to framework-building coral dominated shallow-water ecosystems is linked to long-term Cenozoic cooling, which enhanced water-column stratification, promoting the development of pycnoclines, and facilitated internal-wave activity (Pomar et al., 2017). These processes increased vertical nutrient transport and plankton availability, favoring suspension feeders, including facultative taxa such as corals. Unlike LBF, corals rely more strongly on particulate organic matter in their heterotrophic mode, and thus benefit from turbulent hydrodynamic conditions that enhance food delivery (Pomar and Hallock, 2007; DeCarlo et al., 2015). The ecologic changes had major consequences for carbonate-platform architecture, promoting margin accretion and the development of coral-dominated buildups.

Throughout the Early and Middle Miocene, coral bioconstructions in many regions of the Mediterranean and Indo-Pacific were typically represented by small, low-relief mounds that developed under oligophotic to mesophotic conditions, except during specific intervals (Danian, Bartonian–Priabonian, Rupelian and Chattian) when larger coral mounds formed (Pomar et al., 2017; Bosellini et al., 2025). Only after the Middle Miocene Climatic Optimum (MMCO), particularly from the late Tortonian onward, large euphotic reef systems became widespread, associated with further cooling and the upward migration of corals towards shallow, warmer-water refugia (Pomar and Hallock, 2008). This transition reflects a reorganization of coral ecosystems and symbiotic relationships under changing thermal and light regimes, facilitating the emergence of better-adapted clades of the symbiotic zooxanthellae of corals (*Symbiodinium*; Pochon et al., 2006; Pomar and Hallock, 2008).

Within this global ecological reorganization, the Miocene coral deposits of the Red Sea are of specific interest. The opening of the Red Sea as a narrow, semi-restricted basin, coeval with the fragmentation of the Tethys, created oceanographic conditions distinct from those of the open Indo-Pacific and Mediterranean provinces (Perrin, 2002; Bosworth et al., 2005; Torfstein and Steinberg, 2020; Öğretmen et al., 2025). Reduced seawater exchange, potential differences in hydrochemistry, and biogeographic filtering may have influenced the timing, composition, and ecological functioning of early coral communities in this basin (Perrin et al., 1998; Pisapia et al., 2024). Yet, despite taxonomic and sedimentological descriptions of Miocene coral occurrences along the Red Sea margins, their role within the broader Miocene coral expansion and their paleoecological significance remain poorly constrained.

Here we present the first paleoecological investigation of the southernmost known Miocene coral-dominated deposits in Saudi Arabia. Based on detailed outcrop descriptions, stratigraphic logging, drone-based mapping, taxonomic identification of foraminifera and

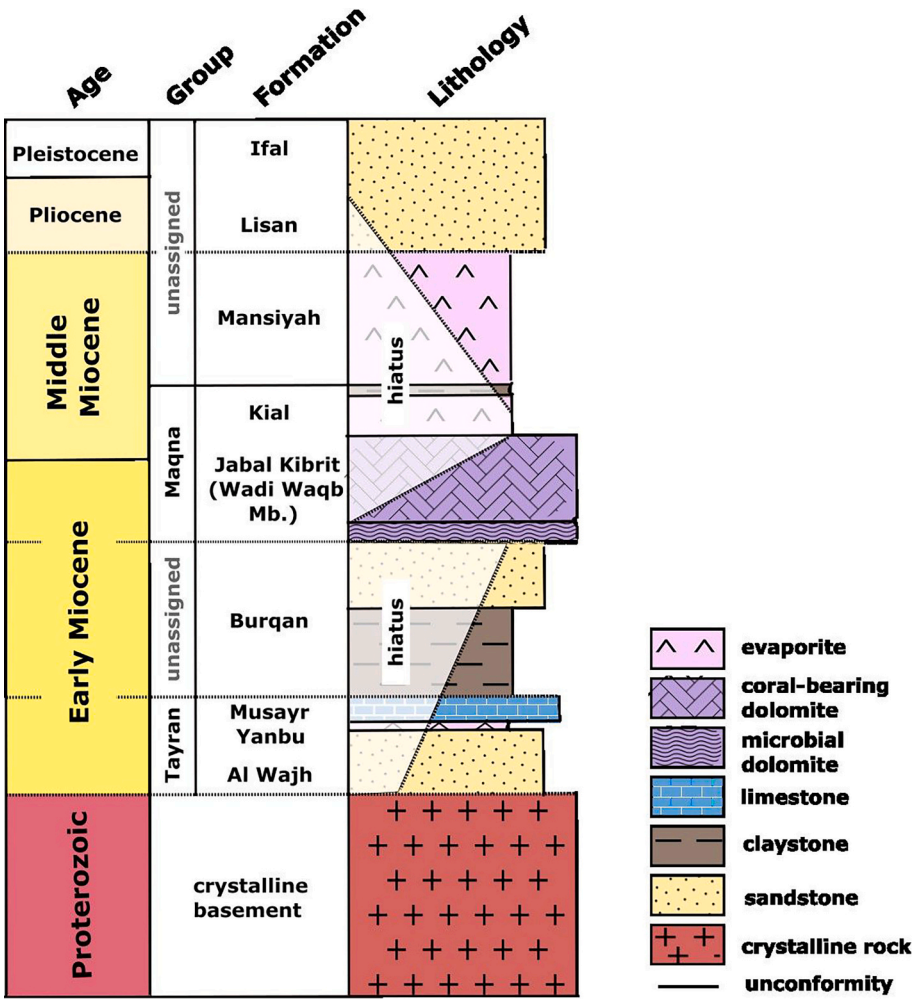

Fig. 2. Schematic stratigraphy of the study area (after Hughes, 2014).

associated organisms, and facies analysis, we develop an ecological model for the earliest coral bioherms in the incipient Red Sea. By comparison with coeval systems from the Mediterranean (Brandano et al., 2016; Pomar et al., 2017), we place these deposits in the context of the Miocene ecological transition from LBF-dominated to coral-dominated carbonate factories.

1.1. Study area

Rifting of the Red Sea basin commenced during the early Oligocene, followed by a second rapid rifting phase taking place in the Late Miocene (Augustin et al., 2021; Rasul et al., 2015; Camp and Roobol, 1992; Stern and Johnson, 2019). The extensional tectonics led to the formation of half-graben structures (Stephen et al., 2005; Tubbs et al., 2014). Early sedimentation in the north of the rift graben during the late Oligocene to Early Miocene (Chattian M–Aquitanian) consisted of thin continental red beds, overlain by Aquitanian (ca. 23–20 million years ago, Ma) shallow to marginal marine conglomerates, sands, and mudstones that spread further south (Hughes and Johnson, 2005). In the Burdigalian (roughly 20–15 Ma), the first marine incursion in the Red Sea took place through the connection to the Mediterranean (Bosworth et al., 2005; Segev et al., 2017), as reflected by synrift sediments consisting of *Globigerina* marls and shales in the central rift basins (Hughes and Johnson, 2005). The coral buildups of the Wadi Waqb Member have been interpreted to have developed along the footwall margins of rotated basement blocks related to the rifting of the Red Sea (Pensa et al., 2025a). First coral taxa invaded the Red Sea during the Burdigalian from the Mediterranean (Pisapia et al., 2024), leading to carbonate deposition along the northern Red Sea shores (Pensa et al., 2025, 2025b). The coral bioherms disappeared again during the late Serravallian (<12 Ma) when the Red Sea was isolated from the open ocean through tectonic movements, closing the connection to the Mediterranean, as reflected by km-thick evaporite successions deposited in the rift sub-basins (e.g., Orszag-Sperber et al., 1998). This salinity crisis set in roughly ten million years earlier than the Messinian salinity crisis in the Mediterranean at ca. 6–5 Ma (Bosworth et al., 2020; Torfstein and Steinberg, 2020; Pensa et al., 2025). In the Pliocene (ca. 5–3 Ma), normal marine conditions were restored with a newly established connection to the Indian Ocean via the Bab-al-Mandab (McClay et al., 1998), while the connection to the Mediterranean via the Gulf of Suez remained closed by tectonic uplift (Bosworth et al., 2020).

Along the Saudi Arabian Red Sea coastline, the coral-rich carbonate unit of the Wadi Waqb Member (Jabal Kibrit Formation) extends in discontinuous outcrops stretching from the northern Midyan area in to the southern reaches of the Gulf of Aqaba (Fig. 1A), to the area of Umluj where the study area is located (Hughes and Johnson, 2005; Hughes, 2014; Al-Kahtany, 2017; Pensa et al., 2025) (Fig. 1). As visible on satellite images along the northern Red Sea coast, the carbonates of the Wadi Waqb Member wrap around the morphology of the paleo-shoreline of northern Saudi Arabia (Pensa et al., 2025, 2025b). This depositional environment received abundant siliciclastic sediments eroded from the uplifted basement at the graben shoulders (Hussain and Al-Ramadan, 2009). The stratigraphic description of the Miocene of the Saudi Arabian Red Sea coast is largely based on the Midyan area in the

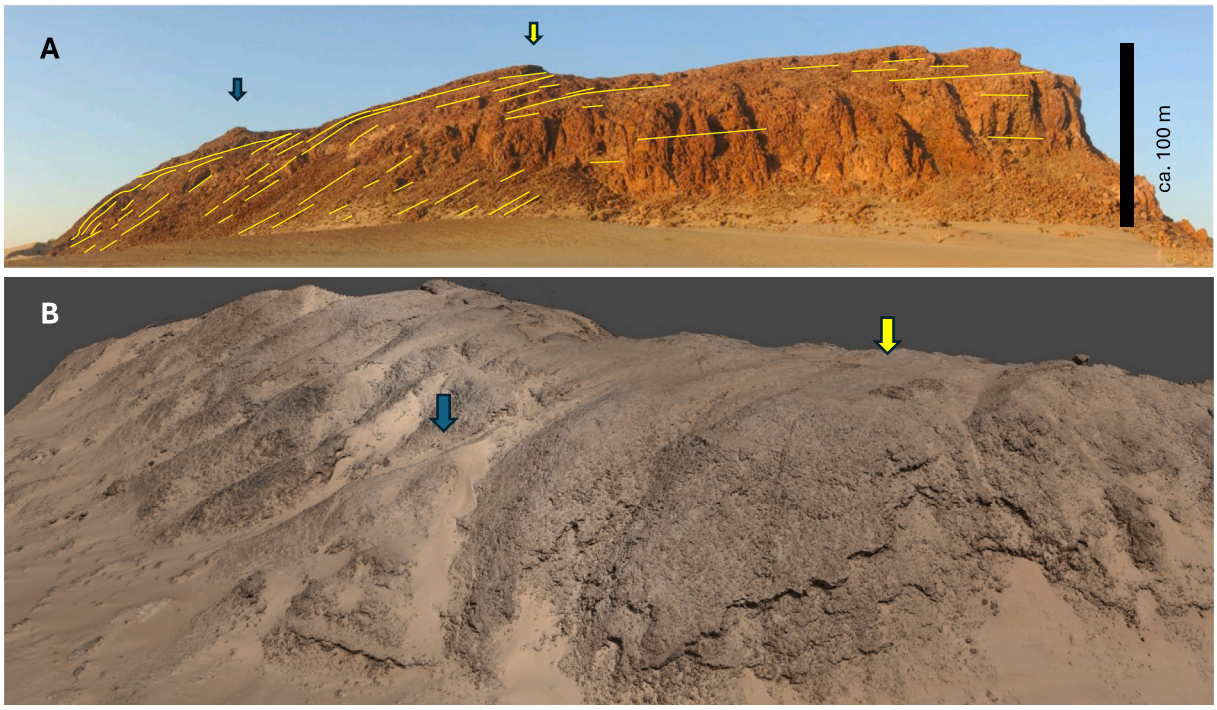

Fig. 3. Umluj site, prograding clinoforms (ca. 20°) towards the modern Red Sea. (A) Photographic panorama taken from the wadi looking north, height of outcrop ca. 100 m. Yellow lines indicate depositional surfaces. (B) Drone image of the front of the prograding ramp illustrating the stacked clinoforms. Blue and yellow arrows point to the same spots in (A) and (B) for orientation. (For interpretation of the references to colour in this figure caption, the reader is referred to the web version of this article.)

North of Saudi Arabia (Fig. 2; e.g., Hughes and Johnson, 2005; Pensa et al., 2025), with limited paleoecological interpretation inferring warm-water conditions within the photic zone based on the coral assemblage (but see El-Sorogy et al., 2020).

Studies on the Wadi Waqb Member in the Midyan area at the northern Red Sea coast of Saudi Arabia have pointed to a Burdigalian age (Al-Kahtany, 2017; Hughes, 2014; Hughes and Johnson, 2005; Hussain and Al-Ramadan, 2009). The carbonates unconformably overlie crystalline basement assigned to a Precambrian age, and siliciclastic sediments assigned to the Early Miocene Al-Wajh Formation (Al-Kahtany, 2017) (Fig. 1D). The Midyan area has been strongly affected by tectonic movements, causing both, syn- and post-sedimentary disruption of the coral-rich carbonates. Magmatic activity locally has led to hydrothermal overprint (Hughes, 2014).

The coeval outcrops studied here are located in the foot-hills west to the flanks of the uplifted mountain range delineating the Red Sea basin north of Umluj (25°33′20.5"N, 37°07′25.7"E to 25°07′54.0"N, 37°24′04.2"E; Fig. 1A). The northern site, here informally termed "Al Wajh site", covers outcrops sticking out of modern desert dunes, forming a double-S shape (Fig. 1B). The second site to the south, here informally named "Umluj site", features an outcrop of the carbonate to the west of the basement that is cut in dip direction by a fault-controlled wadi (Fig. 1C).

2. Methods

Field work at the Al Wajh and Umluj sites took place in 2022 and 2023. After reconnaissance and photographic documentation of the outcrops, we examined and documented the stratigraphy and the geometries of the outcrops in detail (for geographical coordinates see Supplementary Table 1), and collected samples for subsequent microfacies, taxonomic, and mineralogic analyses. Stratigraphic sections were logged where outcrop conditions permitted. In March 2023, two unmanned aerial system (UAS) surveys were conducted with the support of the company FalconViz, covering 0.25 km^2 and 0.52 km^2 for the Al Wajh and the Umluj sites, respectively (Fig. 1C, D). Photos were captured using a DJI Zenmuse P1 45-megapixel camera (resolution of 8192 × 5460 pixels). In total, 5257 and 12,380 photos were captured at the Al Wajh and Umluj sites, respectively. Using Agisoft Metashape Professional (v. 2.1.0 build 17,532, Agisoft LLC © 2023), we created digital twins of each outcrop following a standard Structure from Motion/Multi-View Stereo (SfM/MVS) workflow for drone data (e.g., Scardino et al., 2025). From the digital twins, digital terrain models and georeferenced orthomosaics were also created. Orthomosaics and quality reports for each outcrop are provided in the Supplementary Material 1 and 2. In order to assess overall distribution of coral mounds and bioherms across each outcrop, we manually annotated each orthomosaic in QGIS (v. 3.40.4). The positional data to all references are available in Supplementary Table 1.

Facies definition and description is based on field observations complemented by thin section analyses. A total of 150 thin sections were prepared for microfacies and taxonomic analyses, polished to 40 μm thickness. We followed the Dunham (1962) for classification of texture as modified by Insalaco (1998). The generic and suprageneric classification of foraminifera follows Loeblich and Tappan (1987). For corals, we use the taxonomic identification previously published on one of the outcrops studied here as part of the same larger project (Pisapia et al., 2024).

X-ray diffraction (XRD) was conducted in the laboratories of the Crystallography and Geomaterials Research Group of the Department of Geosciences, University of Bremen. Dried bulk samples were ground to a fine powder (<20 μm particle size) and prepared with a Philips backloading system. For XRD analysis, a Bruker D8 Discover diffractometer was used. The instrument was equipped with a Cu-tube (k_α 1.541 Å, 40 kV, 40 mA), and a fixed divergence slit of ¼°, a monochromatization via energy discrimination on the highest resolution Linxeye detector system. The measurements have been done as a continuous scan from 3 to 65° 2θ, with a calculated step size of 0.016° 2θ. Mineral identification was done with the Philips software X'Pert HighScore™ Vs. 1.2 (Degen et al., 2014). The determination of well crystallized minerals like quartz,

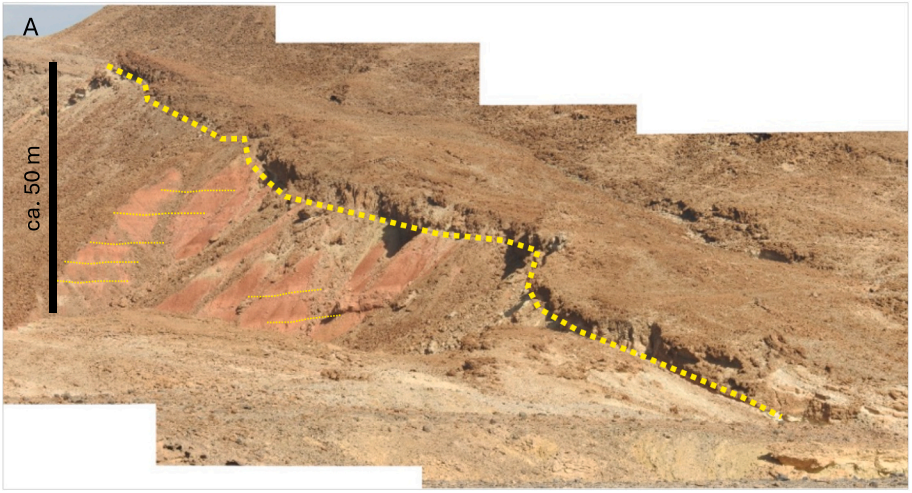

Fig. 4. Photograph of the Al Wajh site (left is N, right is S), showing the contact between horizontal siliciclastics (below) and lowermost sediments of the Wadi Waqb Member carbonates (atop), here: microbialites. Bold yellow dashed line indicates unconformity at the base of the Wadi Waqb Member; thin yellow dashed lines illustrate the bedding of the underlying siliciclastic sediments. (For interpretation of the references to colour in this figure caption, the reader is referred to the web version of this article.)

calcite or aragonite has a standard deviation of ±1–3% (Hardy and Tucker, 1988; Vogt et al., 2002).

3. Results

3.1. Depositional architecture

The Wadi Waqb Member (Fig. 3) is generally well exposed in the study area, with outcrops vertically extending over about 100 m. The outcrops are locally disturbed by tectonic fracturing producing brecciated sections. The exposure is spatially limited upslope by erosion and downslope by a cover of modern sand dunes.

In the study area, the base of the Wadi Waqb Member consists of fine-grained dolomitic microbialites, discontinuously draping an erosional paleo-coastal morphology (in particular the double-S shape at the Al Wajh site: Fig. 1B). Where the contact is visible, the Miocene carbonate sediments rest unconformably on siliciclastic sediments or Precambrian basement (Fig. 2). At the Al Wajh site, horizontally bedded red siliciclastics are exposed beneath the unconformity (Fig. 4), indicating minor if any potential post-depositional tectonic inclination. At the Umluj site, the contact between the sedimentary basement and the overlying succession of prograding clinoforms of the Wadi Waqb Member is exposed along dip direction in a modern wadi (Fig. 1C). The fine-grained microbial carbonates grade upward into the coral-dominated carbonate unit studied here.

Overall, the carbonate outcrops at both sites show the geometries of a distally steepened ramp with the slope showing abundant amalgamated in situ coral mounds embedded bioclastic debris with abundant coral rubble. The individual prograding clinoforms formed by this sediment are up to a few meters thick and dip basinwards at ~20° (Fig. 3). The drone imagery reveals that on the upper slope the coral colonies on the carbonate ramp slope cover more area and get more elongated along strike direction (Fig. 5).

3.2. Section logs, outcrop descriptions, and facies

The different outcrops have been investigated by means of detailed stratigraphic logging and facies and microfacies analysis. Rock textures have been described, and the main components forming the carbonate factory have been identified.

The morphology of the coral colonies varies significantly with depth at both sites. In both sites, stratigraphic section logs reveal that the coral colonies, mainly poritids, have higher profiles (up to 3 m) on the lower slope where they form amalgamated stacks, while the elongated chains of colonies towards the upper the ramp are characterized by a low profile (about 1 m). Notably, larger massive to columnar *Porites* colonies dominate the lower part of the succession, whereas colonies of various taxa (*Dipsastrea*, *Diploastrea*, *Favites vasta*) are present in the upper part of the slope profile, with *Cyphastrea serailia* forming extensive flat colonies at the top (for taxonomic identification of the corals from these outcrops, see Pisapia et al., 2024). Sediment between coral mounds contain skeletal grains from shallower-water settings (e.g., *Halimeda* plates, epiphytic foraminifera, ooids, and articulated red algae), mesophotic components (rhodoliths and crusts of red algae, nummulitids, and *Amphistegina*) as well as components from open marine environments (planktonic foraminifera).

Based on outcrop observations and thin section analyses, a total of four coral-related carbonate facies were distinguished (Table 1): coral boundstone (Facies CB), calcareous-algal dominated packstone (Facies CAP), coral floatstone (Facies CF) and bivalve-rhodolith rudstone to floatstone (facies RBF-R). Facies CB and CF are subdivided into subfacies CBpl and CFpl (with planktonic foraminifera) and subfacies CBnpl and CFnpl (without planktonic foraminifera).

3.3. Al Wajh site

The sections AW3, AW4 and AW6 are located in the southern part of the Al Wajh site. Sections AW3 and AW4 are covered by the drone survey (Fig. 1B). The taxonomic identification of corals in the AW4 section has been previously published as part of the larger project (Pisapia et al., 2024), showing a dominance of poritids and a generally low diversity with 10 taxa identified to genus or species level. The sections AW3 and AW4, part of the same outcrop, are separated by a fault and are parallel sections along dip direction.

3.3.1. Section AW3 (Fig. 6)

Below section AW3, a largely covered basal microbialite layer is present that is not included in the logged section. Above, section AW3 begins with a 13.7 m thick succession of carbonate deposits characterized by coral bioherms forming mounds; hence, corals and associated skeletal grains are prominent components. The basal 2.9 m of the AW3 section comprise coral bioherms forming mounds embedded in a fine-grained matrix (facies CB, subfacies Sf CBpl). In the lower portion, the inter-mound facies consists of a wackestone-packstone rich in red algal

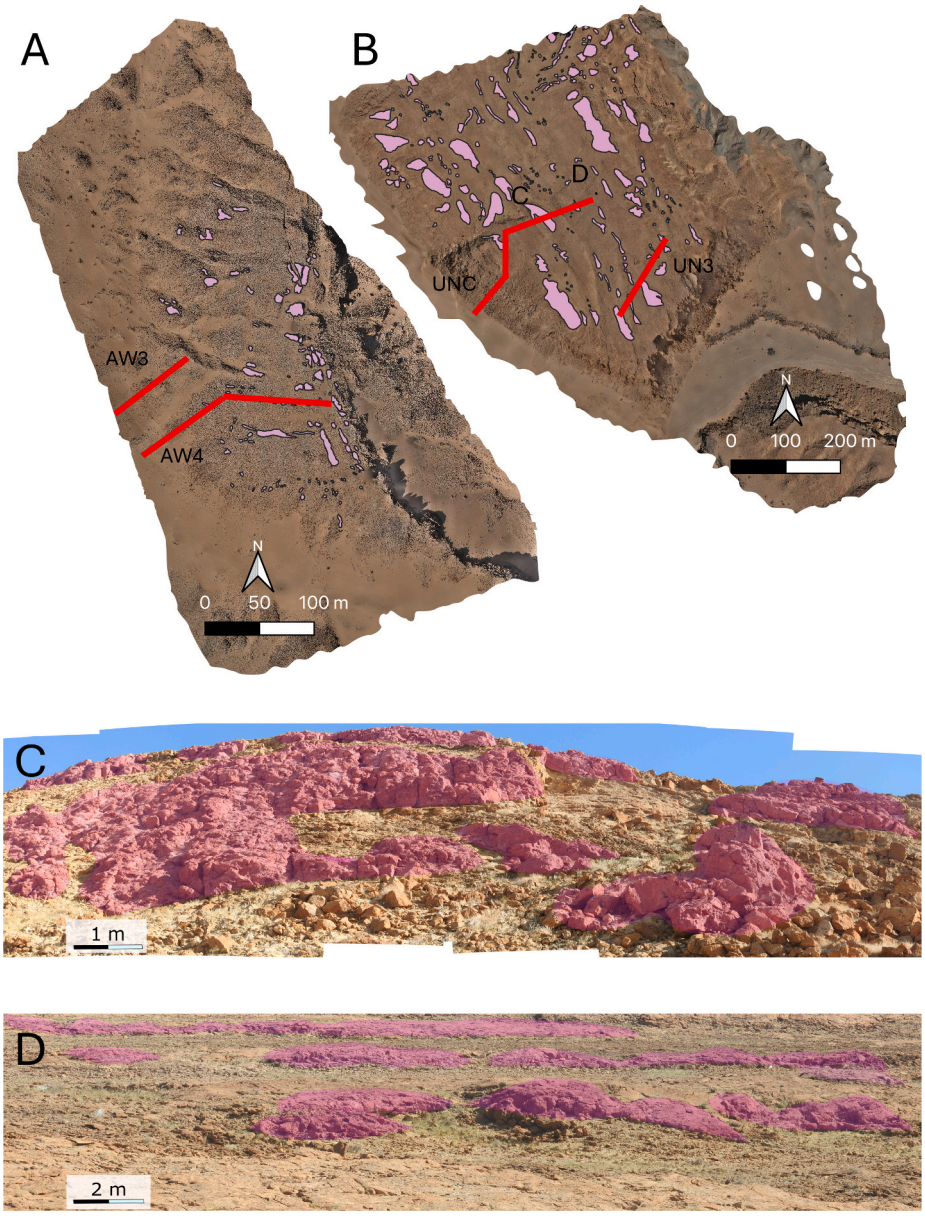

Fig. 5. (A) Orthomosaic of the Al Wajh site indicating the distribution of the exposed coral framestone, as well as of the logged sections AW4 and AW6. (B) Orthomosaic of the Umluj site indicating the distribution of the exposed coral mounds, of the logged sections UNC and UN3, as well as of the close-ups shown in C and D. (C) Close-up of coral framestone near the top of the UNC section. (D) low-relief coral mounds on top of the Umluj outcrops.

fragments, *Halimeda* ghosts, and benthic foraminifera, including encrusting acervulinids and *Planorbulina*, along with planktonic foraminifera. Section upwards, the inter-mound facies grades into a grainstone-packstone with a more diverse assemblage of grains, including echinoderms, decapods, articulated and non-articulated red algae (including *Mesophyllum*) and bryozoans. Coral preservation is variable; *Porites* skeletons appear largely dissolved, however, they are indicated by crusts of red algae typical for encrusting corals. Benthic foraminifera include encrusting taxa (e.g., victoriellids and *Nubecularia*), large symbiont-bearing benthic genera (hyaline: *Operculina, Heterostegina* and *Amphistegina*; porcelaneous: *Peneroplis*), as well as small benthic taxa (e.g., *Cibicides* and miliolids such as *Quinqueloculina*). The planktonic foraminiferal assemblage includes specimens referred to the genera *Trilobatus*, *Praeorbulina*, and *Globigerinoides*. The deposits show evidence of dolomitization and moldic porosity, and some parts of the outcrop are covered by modern debris.

Above this level, between 2.9 and 8.0 m, coral mounds continue to be present; however, poor preservation limits paleoecological interpretation. The available evidence suggests a predominance of *Porites* mounds between 4.7 and 7.4 m. Large portions of this interval are covered by modern debris.

A more distinct coral mound facies emerges at 8.2 m, where the inter-mound facies is more heterogeneous, consisting of a wackestone-grainstone (Sf CBpl). The skeletal assemblage is highly diverse, featuring corals encrusted by red algae, red algal branches, bivalves, decapods, echinoderms, and branching bryozoans. Benthic foraminifera are diverse and include small miliolids (e.g., *Pyrgo*, *Spiroloculina*), small epiphytic taxa (e.g., *Cibicides*, *Lobatula*), and forms encrusting corals (e.g., *Sphaerogypsina*, *Miniacina*). Notably, the symbiont-bearing genus *Peneroplis* occurs associated with *Planorbulina* and *Textularia*. Small planktonic foraminifera (including *Globigerinoides ruber*, possibly *Trilobatus sicanus*) are abundant. Scattered quartz detritus is present.

Towards the top of the section (from 11.8 to 13.7 m), preservation of the skeletal grains becomes poorer. The facies of the uppermost deposits

Table 1
Facies described from Al Wajh and Umluj localities, based on the textural and compositional features determined qualitatively.

Facies	CB	CAP	CF	RBF-R
Subfacies	Sf CBpl (planktonic foraminifera present, ooids present), Sf CBnpl (planktonic foraminifera absent)	N/A	CFpl (planktonic foraminifera present), CFnpl (planktonic foraminifera absent)	N/A
Texture	Coral boundstone (large mounds) with inter-mound sediment (wackestone to packstone/ grainstone)	Packstone	Coral floatstone with wackestone to packstone matrix	Floatstone to rudstone with large bivalves (possibly cardiids) and rhodoliths within a grainstone matrix
Components	Dominant In situ coral colonies (mainly *Porites*). Abundant Articulated and non-articulated red algae (including genera *Sporolithon* and *Mesophyllum*). Green algae (*Halimeda*) Frequent Echinoderms, bivalves, gastropods, ostracods, decapod crustaceans, bryozoans, serpulids Benthic foraminifera: Symbiont-bearing Large hyaline: *Operculina, Heterostegina, Amphistegina*. *Miogypsina globulina* (only in UN7 section) Large porcelaneous foraminifera: *Peneroplis, Dendritina, Archaias, Borelis melo, B. curdica* Small benthics: *Textularia*, *Cibicides*, small miliolids (*Quinqueloculina, Spiroloculina, Pyrgo*) Encrusting foraminifera: acervulinids, victoriellids, *Nubecularia, Sphaerogypsina, Miniacina, Planorbulina.* Planktonic foraminifera (Sf CBPL) *Praeorbulina, Globigerinoides ruber, Trilobatus sicanus* Rare Quartz grains Ooids	Dominant Fragments of non-articulated red algae, green algae (*Halimeda* plates) Abundant Serpulids, bryozoans, echinoderms, gastropods, bivalves (including oysters heavily bored by *Entobia*) Encrusting foraminifera: victoriellids Planktonic foraminifera: Globigerinids such as *Trilobatus trilobus, T. bisphericus, Praeorbulina glomerosa, Globigerinoides subquadratus* Frequent Benthic foraminifera: Symbiont-bearing Large hyaline: *Operculina* Large miliolids: *Borelis* (*B. melo* and *B. curdica), Peneroplis* (including *P. evolutus*), *Spirolina, Dendritina* Small benthics: discorbids, *Rosalina*, *Cibicides*, *Textularia* Rare Quartz grains	Dominant Coral fragments Abundant Non-articulated red algal crust fragments (*Mesophyllum*), Frequent *Halimeda* plates, gastropods, bivalves, solitary corals, ostracods, serpulids, articulated red algal fragments *Gastrochaenolites* borings Benthic foraminifera Symbiont-bearing Large porcelaneous foraminifera: *Peneroplis*, *Spirolina, Borelis, Sivasina* Small benthics: *Cibicides*, *Elphidium*, small miliolids (*Quinqueloculina, Triloculina, Pyrgo*) Encrusting foraminifera: victoriellids (*Biaritzina*), *Miniacina*, *Planorbulina*, acervulinids (including *Gypsina*). Planktonic foraminifera (CFpl) Rare Quartz grains	Dominant Large bivalves (possibly cardiids) Abundant Non-articulated red algae forming crusts and rhodoliths (including genera *Neogoniolithon, Lithoporella, Spongites*). Coral (including *Porites*) Frequent Articulated red algae, echinoderms, molluscs. Benthic foraminifera Symbiont-bearing Large hyaline: *Amphistegina* Large porcelaneous foraminifera: *Peneroplis, Borelis* Small benthics: *Neorotalia, Elphidium*, small miliolids (*Quinqueloculina, Triloculina, Pyrgo*) Encrusting foraminifera: *Acervulina, Miniacina, Victoriella.* Rare Planktonic foraminifera Quartz grains

is a highly heterogeneous coral-*Halimeda* floatstone with packstone matrix (CFpl). Other skeletal components include abundant ostracods and serpulids and benthic foraminifera such as *Planorbulina*, *Cibicides*, and small miliolids, as well as planktonic foraminifera.

3.3.2. Section AW4 (Fig. 7)

The 44.85 m thick AW4 section, although being located close to the fault, exhibits minor brecciation. At the base (0–0.45 m), two layers of floatstone with a fine-grained wackestone-packstone matrix show a skeletal assemblage that mostly consists of coral fragments and bivalves with red algal crust fragments, potentially *Mesophyllum*, and evidence of *Gastrochaenolites* borings (CFnpl).

Between 0.45 and 6.55 m, several stacked coral mounds and inter-mound floatstones can be distinguished (Sf CBpl). The coral surfaces are extensively encrusted by red algae, serpulids, and foraminifera such as victoriellids and homotrematids. The wackestone-packstone matrix of the floatstone consists of coral fragments, particularly *Porites*, red algal nodules and crusts, articulated red algae fragments, *Halimeda* plates, echinoderms, bryozoans, and molluscs, including bivalves (e.g., oysters) and gastropods. The benthic foraminiferal assemblage is diverse, featuring taxa referred to the symbiont-bearing genera (e.g., *Operculina*, *Amphistegina*), small miliolids (*Spiroloculina*), textularids, *Planorbulina*, *Rosalina*, *Elphidium*, and *Cibicides*. The planktonic foraminiferal assemblage includes globigerinids, such as *Praeorbulina glomerosa* and *Globigerinoides ruber*. Some detrital quartz is present.

Between 6.55 and 7.65 m, the deposits transition into a strongly altered, matrix-dominated floatstone with a fine-grained matrix (CFpl). The composition remains similar, featuring red algal nodules and crusts, coral fragments, *Halimeda*, gastropods, and echinoderms. The benthic foraminiferal community includes small miliolids (e.g., *Pyrgo*, *Quinqueloculina*), symbiont-bearing *Operculina* and *Peneroplis*, encrusting homotrematids (*Miniacina*), *Cibicides*, and *Textularia*. The planktonic assemblage continues to feature globigerinids (including *Trilobatus sicanus*).

From 7.65 to 11.80 m, the deposits are affected by tectonic brecciation, with the uppermost meter being covered by debris. The lithology remains a floatstone with a fine-grained matrix, containing abundant *Halimeda*, coral fragments with red algal crusts, bryozoans, molluscs (bivalves and gastropods) (facies CF, subfacies CFpl). The foraminiferal assemblage includes planktonic globigerinids (including *Praeorbulina glomerosa*), and benthic taxa such as *Cibicides*, small miliolids, and *Textularia*. Some quartz grains and other terrigenous detritus are present.

Between 11.80 and 39.15 m, the succession comprises thick layers with sparse coral colonies (facies CB, subfacies Sf CBpl). The inter-mound sediment predominantly consists of wackestones to packstones, locally evolving into floatstones where coral debris becomes more abundant. The floatstone matrix varies from packstone to wackestone and contains *Halimeda*, gastropods, bryozoans, red algal fragments and crusts (including *Spongites* and *Lithoporella*), articulated red algae (*Jania*), serpulids, echinoderms, oysters, and decapods. *Porites* fragments remain abundant. Encrusting components include foraminifera such as

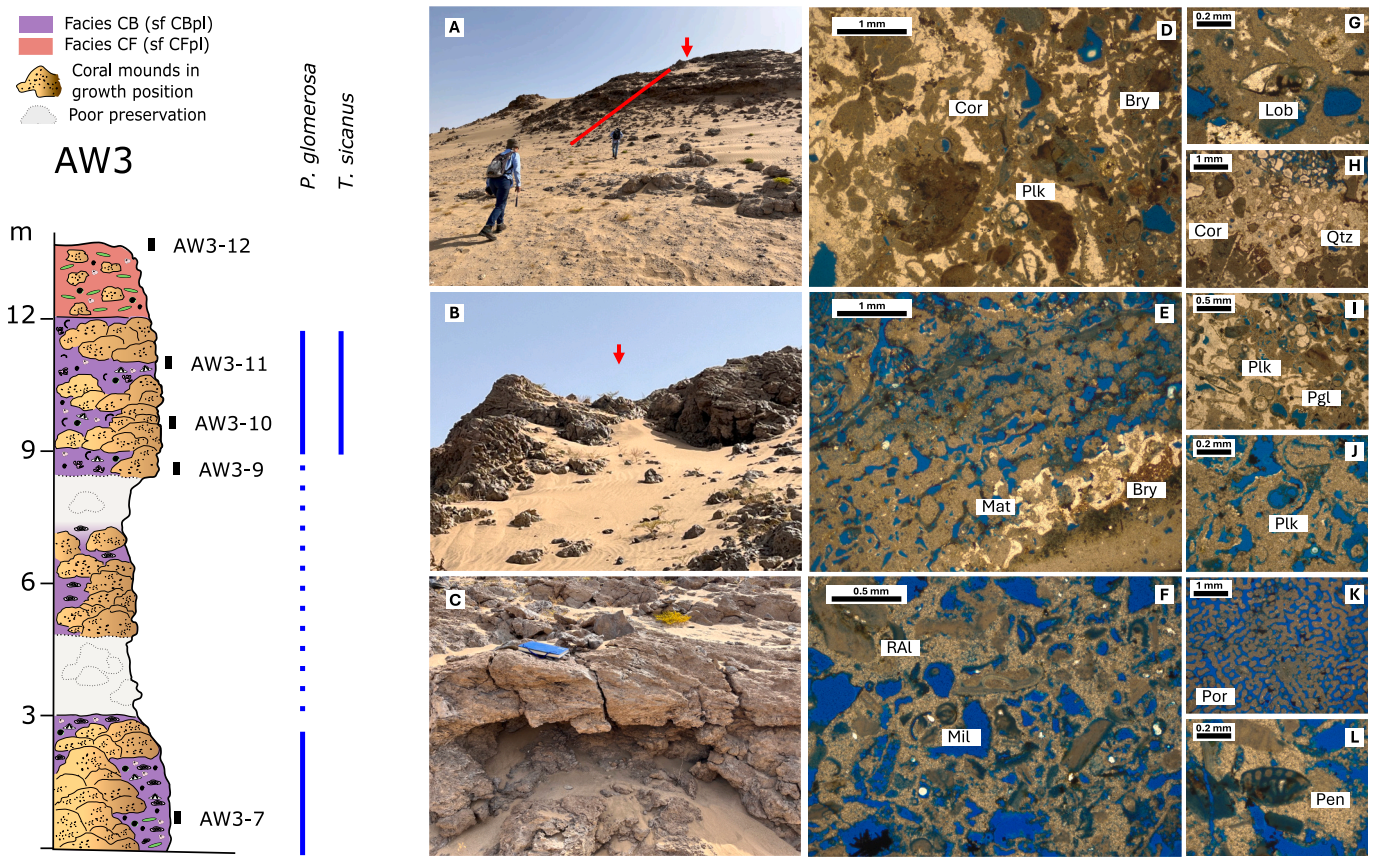

Fig. 6. Stratigraphic log of the facies succession at outcrop AW3, Al Wajh site. Vertical scale in meters. The poor preservation of the grey intervals prevents precise identification of components and textures; however, mold structures attributable to corals can be recognized. (A) Outcrop view showing the logged section indicated by a red line. (B) Upper part of the coral boundstone interval (Facies CB). (C) Coral mold showing sediment infill between colonies. (D) Microfacies (sample AW3–11) corresponding to the coral framework (Cor) forming Facies CB, with encrusting bryozoans (Bry) and planktonic foraminifera (Plk). (E) Microfacies (sample AW3–9) showing sediment (Mat) infilling a poritid coral, including encrusting bryozoans (Bry). (F) Sediments (sample AW3–7) filling spaces between colonies at the base of Facies CB, consisting of packstones to wackestones with a fine-grained matrix (Mat), characterized by abundant dissolved components together with red-algal fragments (RAl) and miliolid foraminifera (Mil). (G) Benthic foraminifer of the genus *Lobatula* (sample AW3–10). (H) Detail of sediment infilling spaces between coral (Cor) colonies, locally containing quartz grains (Qtz) indicative of terrigenous input (sample AW3–10). (I) Planktonic foraminifera (Plk) from packstone to wackestone sediments infilling inter-mound spaces (sample AW3–11), including *Praeorbulina glomerosa* (Pgl). (J) Dissolution features affecting packstone–wackestone facies (sample AW3–9), including molds of planktonic foraminifera. (K) Mold of the coral genus *Porites* (Por) (sample AW3–7), with micritic matrix infilling the corallites. (L) Symbiont-bearing porcelaneous foraminifer of the genus *Peneroplis* (Pen) (sample AW3–7). (For interpretation of the references to colour in this figure legend, the reader is referred to the web version of this article.)

Miniacina, victoriellids, *Acervulina*, and *Sphaerogypsina*. The benthic foraminiferal assemblage includes *Cibicides*, small miliolids, symbiont-bearing *Peneroplis* and possible *Sorites*, and textulariids, while planktonic foraminifera feature *Praeorbulina* sp. and other globigerinids.

In the uppermost interval (39.15 to 44.85 m), the outcrop is characterized by large *Porites* coral colonies forming mounds reaching about 1 m in vertical dimension. The inter-mound sediment is a packstone-wackestone (CFpl), with coral fragments, bryozoans, *Halimeda*, echinoid spines, gastropods, thin red algal thalli, and bivalves. Coral encrustation is present, notably by *Miniacina*. The foraminiferal community includes benthic groups including symbiont bearing genera (*Peneroplis*, *Spirolina, Borelis*), *Elphidium* and small miliolids, as well as planktonic foraminifera. In addition, siliciclastic detritus is present.

3.3.3. Section AW6 (Fig. 8)

The AW6 section exhibits a 63.5 m thick succession dominated by coral colonies, encrusting red algae, and foraminifera, with strong diagenetic overprint (dolomitization) and tectonic brecciation.

The basal 0–4.9 m interval is highly fractured and brecciated, showing strong diagenetic alteration (recrystallization). The matrix consists of wackestone-packstone, transitioning into brecciated floatstone (facies CF, subfacies CFpl). Skeletal components are scarce and include benthic foraminifera (miliolids), solitary corals, and articulated red algal fragments. Dolomitized *Porites* fragments are encrusted by foraminifera such as victoriellids (*Biaritzina*) and acervulinids (including *Gypsina*). Some planktonic foraminifera and poorly sorted quartz grains are present.

Between 4.9 and 5.7 m, the section is composed of tectonic breccia with *Porites* fragments. The 5.7–7.9 m interval is covered by debris. From 7.9 to 8.5 m, floatstone with a wackestone matrix (facies CF, subfacies CFpl) prevails that is strongly diagenetically altered, showing recrystallization and some black impregnation. Bioclasts include gastropods, bivalves, and benthic foraminifera, including *Peneroplis* and miliolids.

The 8.5–25.05 m interval is dominated by coral colonies forming mounds exceeding 2 m in vertical and 5 m in lateral extension, embedded in a packstone matrix (facies CB, subfacies Sf CBpl). Components in the matrix include *Porites* fragments, bivalves, articulated and encrusting red algae (including *Mesophyllum*), serpulids, gastropods, decapods, bryozoans, and echinoid spines. *Halimeda* increases in abundance towards the top, culminating in a *Halimeda* floatstone. Encrusting foraminifera include acervulinids, while other benthic foraminifera are abundant, in particular the symbiont-bearing *Borelis, Sorites, Amphistegina* and *Operculina*, as well as small miliolids (including *Spiroloculina*),

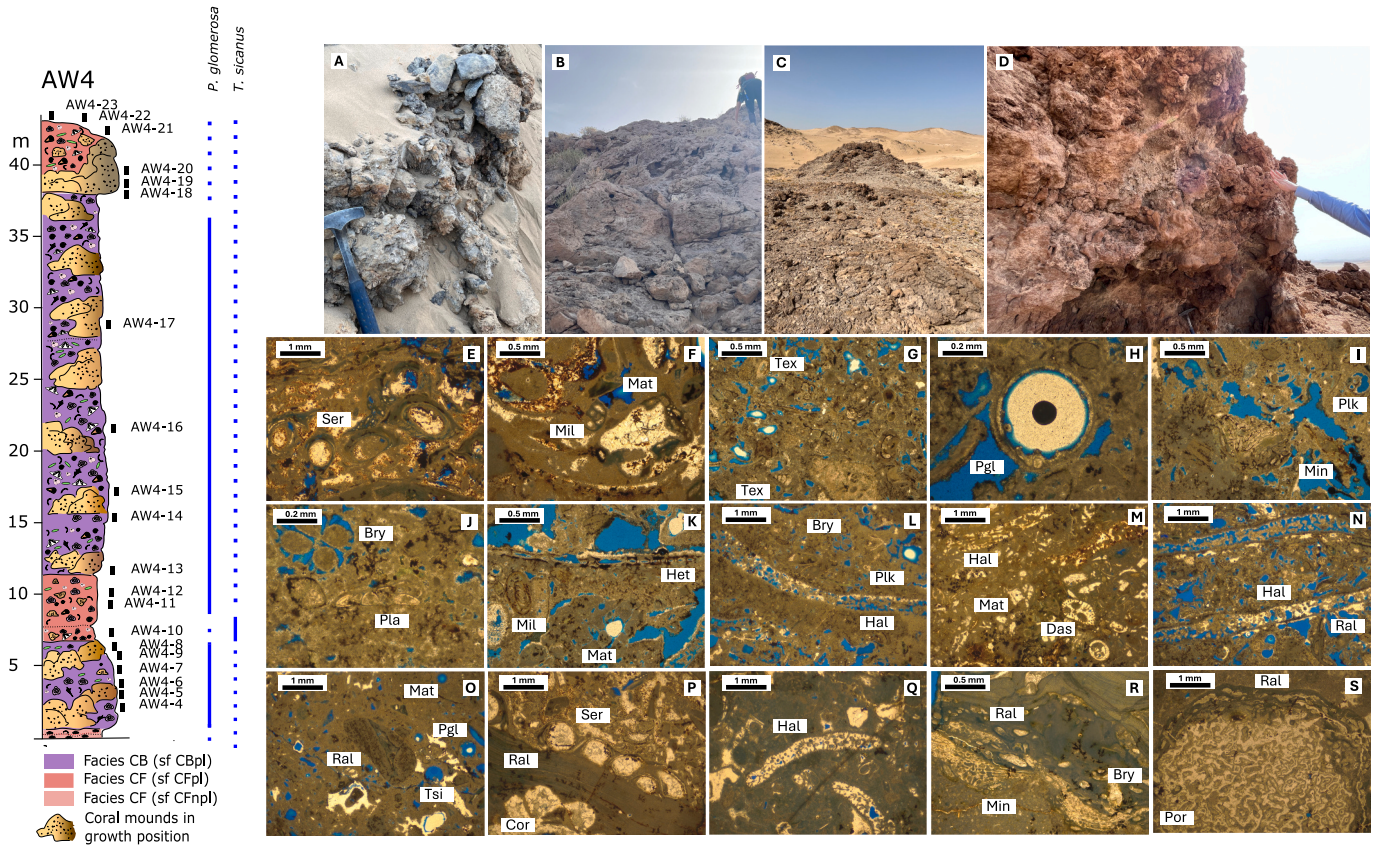

Fig. 7. Stratigraphic log of the facies succession at outcrop AW4, Al Wajh site. Vertical scale in meters. (A) Poorly preserved coral colonies at the top of the lower Facies CB interval. (B) Outcrop view of the upper Facies CB interval. (C) Coral mounds at the top of the section separated by Facies CF. (D) Detail of coral mounds showing partially dissolved colonies. (E–M) Packstone to wackestone sediments filling inter-mound spaces within the lower Facies CB interval. (E) Serpulid worm tubes (Ser) (sample AW4–7). (F) Micritic matrix (Mat) infilling corals and containing miliolid foraminifera (Mil) (sample AW4–7). (G) Packstone grains including benthic foraminifera of the genus *Textularia* (Tex) (sample AW4–8). (H) Detail of the planktonic foraminifer *Praeorbulina glomerosa* (Pgl) (sample AW4–8). (I) Planktonic foraminifera (Plk) associated with the encrusting foraminifer *Miniacina* (Min) (sample AW4–8). (J) Bryozoan fragments (Bry) together with the encrusting foraminifer *Planorbulina* (Pla) (sample AW4–8). (K) Miliolid foraminifera (Mil) and a fragment of the large hyaline symbiont-bearing foraminifer *Heterostegina* (Het) (sample AW4–8). (L) Fragments of the green alga *Halimeda* (Hal), bryozoans (Bry), and planktonic foraminifera (Plk) (sample AW4–8). (M) Green algal fragments, including *Halimeda* (Hal) and dasyclads (Das), within a micritic matrix (Mat). (N, O) Packstone to wackestone sediments forming the matrix of Facies CF. (N) Partially dissolved *Halimeda* (Hal) and red algal fragments (RAl) (sample AW4–10). (O) Red algal fragments (RAl) and planktonic foraminifera, including *Praeorbulina glomerosa* (Pgl) and *Trilobatus sicanus* (Tsi), within a micritic matrix (sample AW4–12). (P—S) Packstone to wackestone sediments filling inter-mound spaces within the upper Facies CB interval. (P) Serpulid worms (Ser) encrusting red algae (RAl), themselves encrusting coral (Cor) (sample AW4–15). (Q) *Halimeda* (Hal) phylloids within a micritic matrix (sample AW4–17). (R) Red algal fragment (RAl) encrusted by bryozoans (Bry) and the encrusting foraminifer *Miniacina* (Min) (sample AW4–18). (S) Fragment of the coral *Porites* (Por) encrusted by red algae (RAl) (sample AW4–18). (For interpretation of the references to colour in this figure legend, the reader is referred to the web version of this article.)

Cibicides, discorbids, *Planorbulina*, *Bulimina*, and *Textularia*. Planktonic foraminifera include *Trilobatus sicanus* and *T. bisphericus*. Some quartz grains are present.

The interval between 25.05 and 26.7 m is strongly diagenetically altered, but some *Porites* colonies embedded in a fine-grained matrix can be identified. The interval from 26.7 to 39.7 m is covered by modern detritus. From 39.7 to 45.9 m, large coral colonies mounds dominate, with inter-mound sediment containing *Halimeda*, articulated and non-articulated red algae (e.g., *Sporolithon*), and peloids (Facies CB, subfacies Sf CBnpl). The benthic foraminiferal assemblage is diverse and includes miliolids, *Peneroplis* (or possibly *Dendritina*), and abundant *Borelis*. The 45.9–47.3 m interval is covered by debris. Between 47.3 and 48.5 m, the deposits consist of poorly preserved packstone containing *Porites* fragments, *Halimeda*, non-articulated red algae, and miliolids.

From 48.5 to 51.3 m, coral colonies increase in size, with individual massive *Porites* colonies reaching up to 2 m in height, forming mounds embedded in a packstone matrix (facies CB, subfacies Sf CBpl). Skeletal components include *Porites* fragments, *Sporolithon*, *Halimeda*, encrusting bryozoans, bivalves, and echinoderms. Benthic foraminifera include miliolids, symbiont-bearing *Peneroplis*, *Sphaerogypsina*, *Textularia*, and *Cibicides refulgens*, while planktonic foraminifera include globigerinids, including *Globigerinoides ruber* and *Trilobatus trilobus*. The 51.3–58.3 m interval is covered by debris.

Between 58.3 and 63.5 m, the section contains sparse coral colonies in a poorly preserved wackestone-packstone matrix (facies CB, subfacies Sf CBpl). Other bioclasts include gastropods, bivalves, and red algal fragments. Notably, ooids are present throughout this interval. The benthic foraminiferal assemblage includes miliolids, symbiont-bearing *Peneroplis* and *Spirolina*, and *Planorbulina*, while planktonic foraminifera include globigerinids, *Trilobatus trilobus*, and *Praeorbulina glomerosa*.

3.4. Umluj site

The Umluj site represents a discontinuous 3 km long outcrop of a prograding ramp that is cut by a wadi, revealing carbonate deposits reaching some 100 m in height. Section UNC is positioned along the slope of the ramp and continues into outcrop UN3 that is the top of the ramp to the north of the wadi; UNC and part of UN3 are covered by the drone survey of the Umluj site; UN7 is the face of the ramp to the south

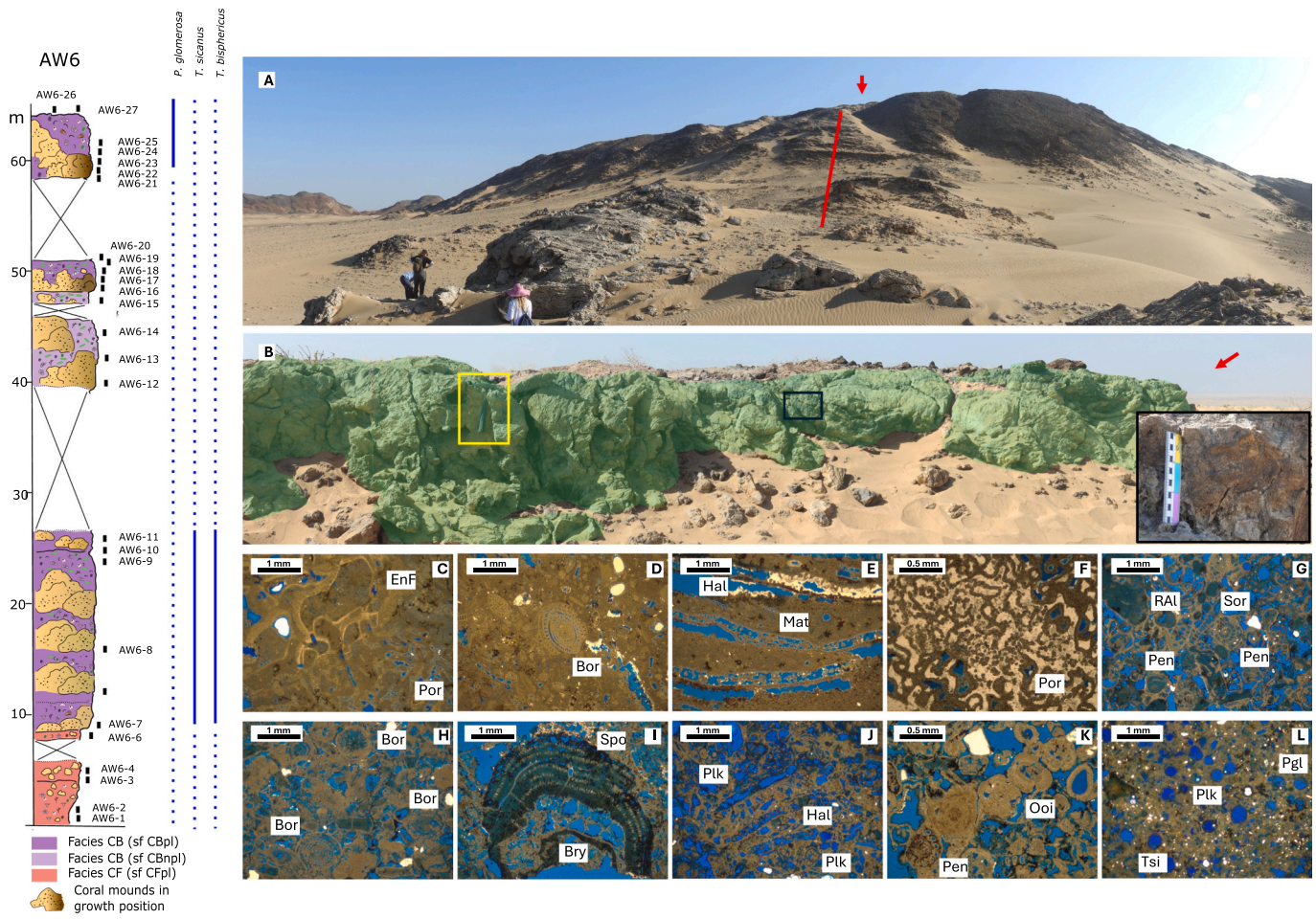

Fig. 8. Stratigraphic log of the facies succession at outcrop AW6, Al Wajh site. Vertical scale in meters; crossed intervals correspond to portions of the section covered by thick debris. (A) General view of the outcrop, with the logged section indicated by a red line. (B) Detail of coral bioconstructions at the top of the section (red arrow); the yellow box outlines a hammer used for scale, and the black box marks a close-up view of the coral colonies. (C) Packstone matrix of the coral floatstone (Facies CF) at the base of the section, showing an encrusting foraminifer (EnF), probably a victoriellid, attached to a poritid coral (Por). (D—F) Packstone to wackestone sediments forming intercolonial deposits of Facies CB in the lower part of the section. (D) Section of the symbiont-bearing porcelaneous foraminifer *Borelis* (Bor) (sample AW6–8). (E) *Halimeda* (Hal) ghosts embedded in a micritic matrix (sample AW6–10). (F) Dolomitized *Porites* (Por) (sample AW6–11). (G–I) Packstone sediments forming intercolonial deposits in the middle part of the section, characterized by intense dissolution affecting skeletal grains. (G) Fragments of red algae (RAl) associated with symbiont-bearing porcelaneous foraminifera of the soritid family (Sor), including *Peneroplis* (Pen) (sample AW6–12). (H) Ghost structures of skeletal grains, including *Borelis* (Bor) (sample AW6–13). (I) Red algal fragment of the genus *Sporolithon* (Spo) encrusting a bryozoan (Bry) (sample AW6–16). (J–L) Packstone to wackestone sediments of Facies CB in the upper part of the section. (J) *Halimeda* (Hal) ghosts associated with planktonic foraminifera (sample AW6–18). (K) Ooids (Ooi) and the foraminifer *Peneroplis* (Pen) (sample AW6–22). (L) Planktonic foraminifera (Plk), including *Trilobatus sicanus* (Tsi) and *Praeorbulina glomerosa* (Pgl) (sample AW6–23). (For interpretation of the references to colour in this figure caption and legend, the reader is referred to the web version of this article.)

of the wadi (for locations see Fig. 1C).

3.4.1. *Section UNC / outcrop UN3 (Fig. 9)*

The section logged on the slope of the ramp (UNC) exhibits a prograding clinoform sequence. The section was logged in the lower part of the outcrop below overhangs that prohibited further upslope logging. Based on the sediment composition, textures and structures, four main facies (CB, including subfacies CBpl and CBnpl; CAP; CF- only subfacies CFnpl; RBF-R) are described.

From 0 to 5.5 m, at the base of the outcrop, facies CB, subfacies CBpl consists of coral colonies embedded in inter-mound sediment corresponding to packstone with frequent *Halimeda*, bivalves, bryozoans, and articulated and non-articulated red algal fragments. Encrusting foraminifera, such as acervulinids, are present, along with benthic foraminifera, including *Planorbulina*, *Cibicides*, and symbiont-bearing *Peneroplis*, as well as planktonic foraminifera, such as *Praeorbulina glomerosa* and *Trilobatus sicanus*.

From 5.5 to 8 m, sediment prevails consists of packstone, which is diagenetically heavily altered at the base (facies CAP). Main components are *Halimeda*, red algal fragments, serpulids, bryozoans, echinoderms, gastropods, and heavily bored bivalves, and oysters with *Entobia* borings. Planktonic foraminifera, such as globigerinids, and encrusting foraminifera, such as victoriellids, are abundant. Nummulitid fragments (*Operculina*), discorbids, *Cibicides*, and *Rosalina*, are also present, along with detrital quartz.

From 8 to 9.5 m, the dominant facies (facies CF, subfacies CFnpl) consists of red algal-dominated floatstone with some coral fragments and packstone matrix with small miliolids and symbiont bearing foraminifera (*Borelis*, *Peneroplis*), serpulid and bryozoan fragments. This facies passes into 1-m thick packstone (facies CAP) with red algal fragments, bryozoans, gastropods, bivalves, serpulids, and echinoderms. Benthic foraminifera include small miliolids and symbiont-bearing *Borelis*, *Peneroplis, Sivasina* (probably *S. egribucakensis*) and *Spirolina*, and *Textularia*. Planktonic foraminifera, such as globigerinids, including *Trilobatus trilobus* and *Praeorbulina* sp., are also present.

The upper part, from 10.5 to 33 m, and presumably above, though

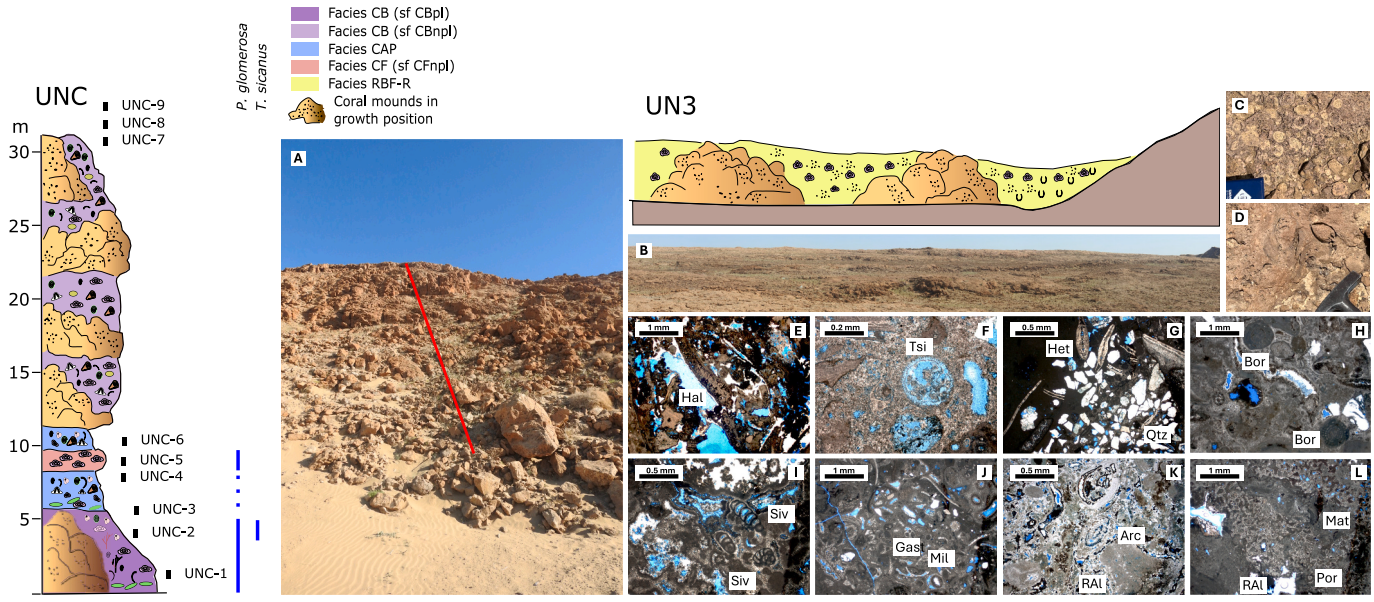

Fig. 9. Stratigraphic log of the facies succession at outcrop UNC and outcrop sketch of UN3, Umluj site. Vertical scale is in meters; the horizontal dimension of the sketch is 30 m. (A) UNC outcrop showing the logged section indicated by a red line. (B) Coral mounds at the UN3 outcrop; sediment filling intercolonial spaces is represented by rhodolith–bivalve rudstone to floatstone with a packstone to grainstone matrix (Facies RBF-R). (C) Detail of rhodoliths corresponding to Facies RBF-R. (D) Detail of bivalves corresponding to Facies RBF-R. (E–F) Packstone to wackestone deposits representing intercolonial sediments of Facies CB. (E) Fragment of the green alga *Halimeda* (Hal) (sample UNC-1). (F) Planktonic foraminifer *Trilobatus sicanus* (Tsi) (sample UNC-2). (G) Packstone (Facies CAP) containing the larger benthic foraminifer *Heterostegina* (Het) and quartz grains (Qtz) (sample UNC-4). (H) Packstone matrix of Facies CF containing *Borelis* (Bor) foraminifera (sample UNC-5). (I) Packstone (Facies CAP) containing *Sivasina egribucakensis* (Siv) (sample UNC-6). (J–L) Packstone deposits corresponding to intercolonial sediments in the upper part of the section (Facies CB). (J) Gastropod fragments (Gas) and miliolid foraminifera (Mil) embedded in a micritic matrix (sample UNC-7). (K) Heavily altered skeletal grains including red-algal fragments (RAl) and symbiont-bearing porcelaneous foraminifera of the genus *Archaias* (Arc) (sample UNC-8). (L) Fragment of the coral *Porites* (Por) encrusted by red algae (RAl) and infilled by micritic matrix (Mat). (For interpretation of the references to colour in this figure caption and legend, the reader is referred to the web version of this article.)

unlogged due to an overhang, the interval is dominated by coral mounds with a packstone-wackestone matrix (facies FA, subfacies Sf CBnpl). Red algal fragments and crusts, including *Mesophyllum*, are present, along with bivalves, gastropods, echinoderms, ostracods, serpulids, and decapod fragments. Foraminifera include encrusting forms, such as *Miniacina*, victoriellids, and acervulinids, as well as benthic forms, including symbiont-bearing *Operculina,* soritids and *Borelis* (including both *B. melo* and *B. curdica*), in association with *Cibicides*, and small miliolids. Planktonic foraminifera were not identified.

The outcrop continues on the top of the prograding ramp as UN3 and in the East of the outcrop reaches the unconformable onlap on the siliciclastic basement. Directly upslope of UNC, section UN3 is characterized by abundant coral mounds creating a large-scale wavy morphology on the progradational foresets dipping westward. The mounds show vertical thickness of less than 1.5 m, and laterally extend over several meters.

Towards the contact to the basement, the top layer of the succession features floatstone to rudstone textures with abundant large bivalves (possibly cardiids), some articulated, and red algal fragments and some rhodoliths within a grainstone matrix (facies RBF-R). Microfacies analysis of the grainstone matrix reveals abundant non-articulated red algae (including *Neogoniolithon, Lithoporella*, and *Spongites*) that locally encrust in situ *Porites* colonies. Other frequent components are articulated algae and echinoderms. Molluscs are also present. Foraminifera identified include benthic forms such as symbiont-bearing *Borelis*, *Peneroplis* and *Amphistegina*, small miliolids (*Pyrgo*, *Triloculina*), *Planorbulina*, *Neorotalia*, and *Elphidium*. Encrusting foraminifera include *Miniacina*, *Acervulina*, and *Victoriella*. Further components include planktonic foraminifera and detrital quartz. The outcrop shows diagenetic impregnation, ranging from pink to black.

3.4.2. *Outcrop UN7 (Fig. 10)*

The UN7 outcrop is tectonically disturbed. At the base of the outcrop, microbialite beds (facies FI) are present, overlain by westward-dipping beds with a dip direction of 260°W. These beds correspond to facies CB, subfacies Sf CBnpl and are characterized by mound structures predominantly composed of coral genus *Porites*, forming dense clusters with individual mounds reaching approximately 1.5 m in thickness. The matrix is fine-grained (packstone to wackestone), and the sediment is poorly sorted and poorly bedded.

The outcrop is generally strongly altered diagenetically, likely due to its proximity to a fault. Above the microbialite beds, the microfacies is very similar, with a fine-grained matrix containing articulated red algae, *Ditrupa*, and other mollusc fragments. *Porites* fragments and siliciclastic detritus are present throughout. The lowermost part of the succession is particularly notable for the very abundant presence of the LBF species *Miogypsina globulina*, which is highly significant for biostratigraphic correlation (see below: 3.6 Age constraints). This association places the succession largely within the Langhian stage of the Middle Miocene.

The outcrop is hypothesized to be stratigraphically below UNC outcrop, representing the earliest colonization phase of the environment.

3.5. *Diagenetic alterations*

Thick sparry calcite veins are present in the outcrops, and in particular towards the top of the succession, black impregnated corals towards the top of the succession in the Al Wajh site are abundant. In thin sections, silica cements are observed in some leached samples.

XRD analyses (Supplementary Table 2) indicate that the carbonates are largely dolomitized (average 75%, minimum 29%, maximum 96%; $n = 23$). In most samples, quartz is very rare (below 5%) or absent; only in very rare cases quartz contents reach 67%.

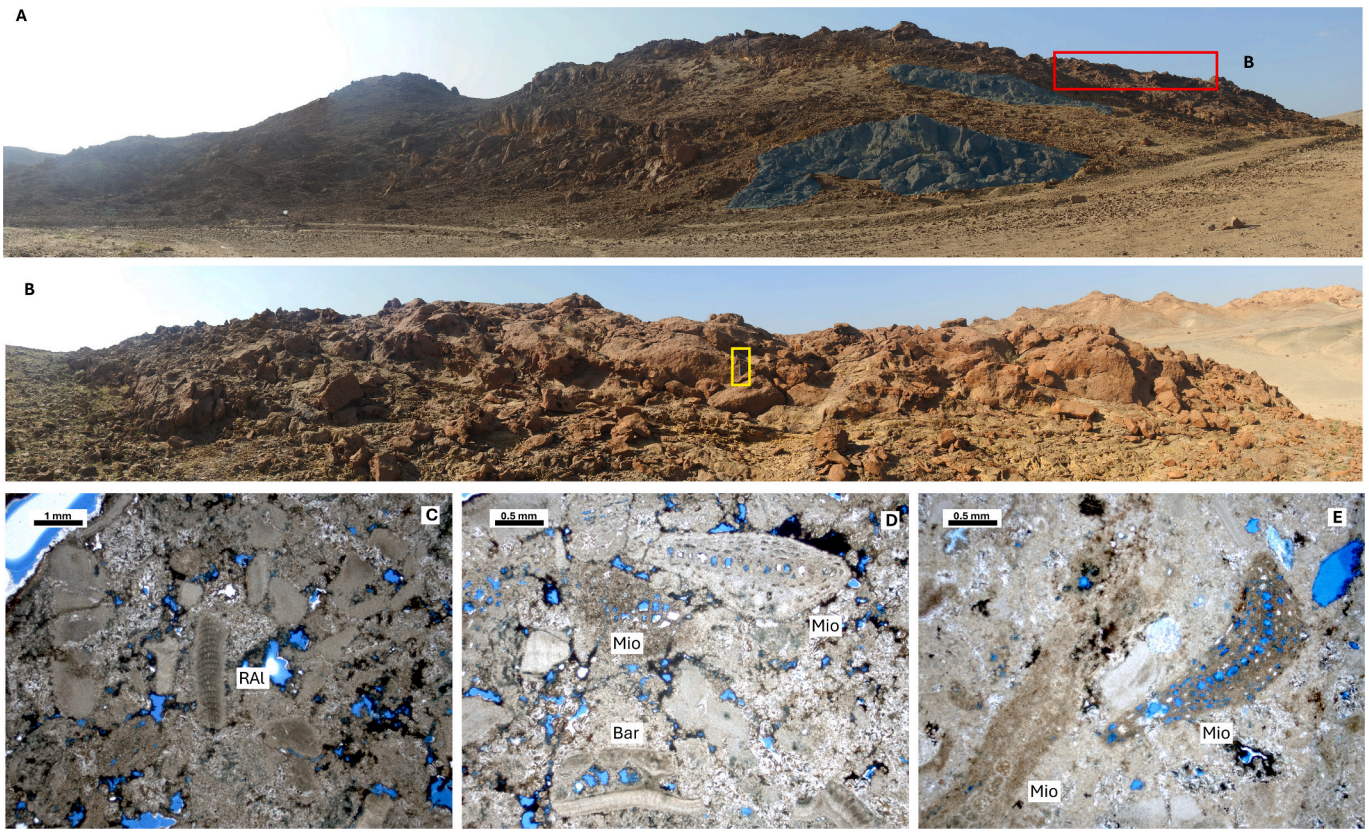

Fig. 10. Outcrop UN7, Umluj site. (A) General view of the UN7 outcrop, with shaded areas highlighting coral mounds. (B) Detail of the upper coral mounds (red box in A); the yellow box outlines a hammer used for scale. (C–E) Heavily altered packstone to grainstone sediments forming intercolonial deposits. (C) Bioclasts including red-algal fragments (RAl) (sample UN7–1). (D) Barnacle fragments (Bar) associated with the larger benthic foraminifer *Miogypsina globulina* (Mio) (sample UN7–1). (E) Detail showing two specimens of *M. globulina* (Mio) (sample UN7–1G). (For interpretation of the references to colour in this figure caption, the reader is referred to the web version of this article.)

3.6. Age constraints (Fig. 11)

The foraminiferal assemblage identified here includes various taxa of significant biostratigraphic relevance. Relevant planktonic foraminifera species identified here include *Trilobatus sicanus*, *T. bisphericus, T. trilobus, Globigerinoides subquadratus*, and *Praeorbulina glomerosa*. According to BouDagher-Fadel (2015), the biostratigraphic range of *T. sicanus* extends from the middle of the N8a biozone to the top of N9b, while *T. bisphericus* spans from the base of N7b to the top of N9a. *T. trilobus* has a broader range, extending from the base of N4b to the present. *P. glomerosa* appears from the base of N8b to the lower part of N9b, whereas *G. subquadratus* extends from the lower part of N4b to the end of N15b. In particular the lowest occurrence of *P. glomerosa* marks the base of the M5b zone sensu Wade et al. (2011), corresponding to the latest Burdigalian.

Observed benthic taxa with biostratigraphic significance that have been identified here include *Borelis melo* and *B. curdica*, along with *Miogypsina globulina*, which is reported here for the first time in the Wadi Waqb Member. *Miogypsina globulina* has only been found in the lowermost part of the Umluj outcrop. As highlighted by Pisapia et al. (2024), a clear faunal affinity existed between the Red Sea and the Mediterranean during the Early and Middle Miocene. Consequently, the stratigraphic distribution of the benthic foraminifera in the studied outcrops follows the pattern observed in the Mediterranean province. The occurrence of *Borelis curdica* in the absence of *B. melo* has traditionally been regarded as indicative of a Burdigalian, or at least pre-Langhian, age (Jones et al., 2006; Hughes, 2014; Yazdi-Moghadam et al., 2018; Roozpeykar et al., 2021). However, recent revisions addressing the systematics, biostratigraphic range, and palaeogeographic distribution of the genus *Borelis* challenge this interpretation (Bassi et al., 2021, 2024). According to these authors, *B. melo* ranges from the Aquitanian to the Messinian, whereas *B. curdica* extends from the lowermost Burdigalian to the end of the Tortonian (Bassi et al., 2021).

In the Mediterranean region, the biostratigraphic range of *Miogypsina globulina* is restricted to the Burdigalian (Drooger, 1993), corresponding to the upper part of planktonic foraminiferal Zone N5b through the end of Zone N7b (BouDagher-Fadel and Price, 2013). A comparable stratigraphic range is also recognized in the Indo-Pacific domain (Drooger, 1993; Briguglio, 2018). Notably, *Sivasina egribucakensis* has been identified in the lower part of the UNC section. This species was originally described by Sirel and Özgen-Erdem in Sirel et al. (2013), subsequently reported from SBZ21–22 A by Serra-Kiel et al. (2016), and later extended up to the Tortonian by Sirel et al. (2020). Moreover, Martín-Martín et al. (2025) recorded its occurrence in SBZ14 (Lutetian), indicating a highly debated and potentially broader stratigraphic distribution.

The age derived from these biostratigraphic constraints for the studied outcrops aligns with other sites where the Wadi Waqb Member has been examined (see Hughes, 2014). As noted by Hughes (2014), the absence of the genus *Orbulina*, along with the reported taxa, supports a transition from the uppermost Lower Miocene to the earliest Middle Miocene. However, the occurrence of *M. globulina* in the lowermost parts of the Umluj outcrop, together with data provided by the poor planktonic assemblages, allows for the first time to constrain the Wadi Waqb Member and thus the first coral colonization of the Red Sea to a latest Burdigalian age.

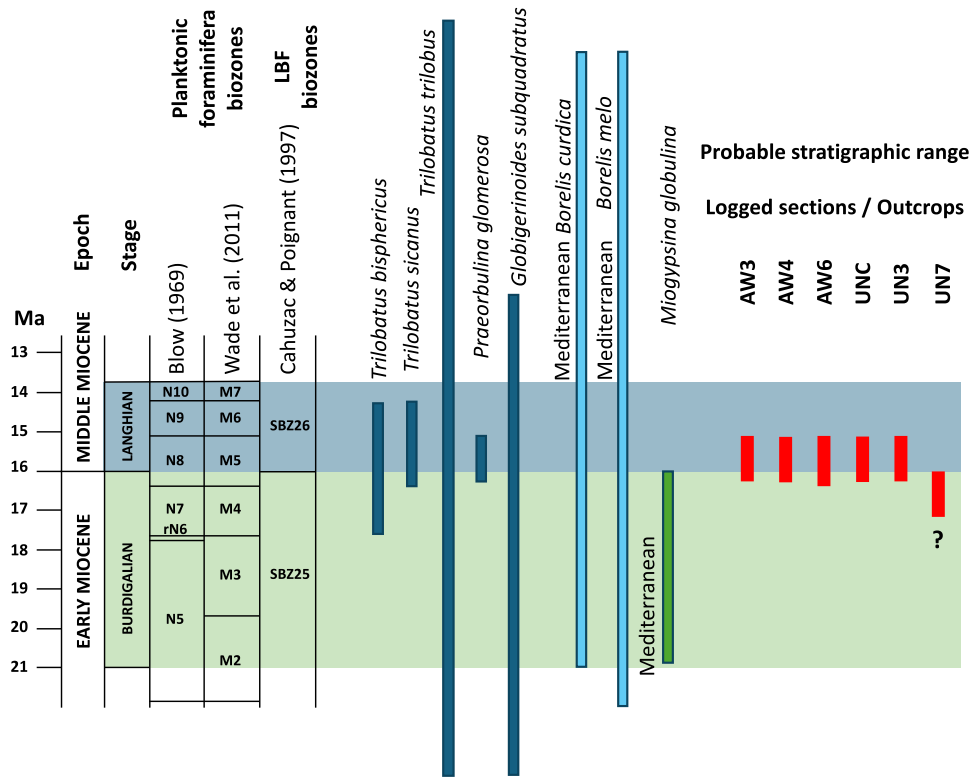

Fig. 11. Stratigraphic range of the most-meaningful stratigraphic markers reported in this study. Planktonic taxa, particularly *Trilobatus bisphericus*, *T. sicanus* and *Praeorbulina glomerosa*, have allowed to place the Al Wajh and UNC and UN3 outcrops in the transition from Burdigalian to Langhian. The occurrence of *Miogypsina globulina* in UN7 indicates a lower stratigraphic position, within the Burdigalian.

4. Discussion

4.1. Outcrop architecture and facies

Field relationships as revealed by drone imagery, as well as sedimentological features observed in the outcrops and through facies analyses, imply that the zooxanthellate coral colonies of the Wadi Waqb Member developed mound-like structures in deeper settings, forming stacked configurations on the depositional slope, while they are arranged into chains parallel to strike on the upper ramp slope (Fig. 10). The geometries observed on outcrop scale exhibit stacked prograding clinoforms (sensu Bosellini, 1984; Quiquerez and Dromart, 2006; Patruno and Helland-Hansen, 2018), dipping basinwards at ~20°. These geometries are consistent with the definition of a distally steepened ramp (sensu Pomar, 2020) and ramp zonations as described in the literature (e.g., Buxton and Pedley, 1989; Pomar et al., 2017) (Fig. 11). Under shallow euphotic conditions - corresponding to the inner ramp -, carbonate production likely occurred within seagrass meadows and ooid shoals, with scattered coral colonies as manifested by epiphytic foraminifera and ooids. Slightly deeper, towards the inner to middle ramp, carbonate production was primarily associated with rhodoliths. In deeper water environments along the slope, sedimentation was characterized by coral mounds that amalgamate into a near-continuous framework, growing on previously stabilized substrates.

This facies zonation compares with other facies models for the prelate Tortonian where corals bioherms did not form rims reaching close to sea level but mostly thrived in meso-oligophotic middle ramp settings, or sparsely occurred in euphotic seagrass-dominated environments (Pomar and Hallock, 2008; Pomar et al., 2017). Between the coral mounds, debris derived from bioherm erosion as well as sediment transported from shallower zones accumulated. The volumetric contribution of the euphotic carbonate factory, however, was minor, and its export downslope was insufficient to mask the mesophotic factory. Accordingly, the Wadi Waqb Member in the study area is interpreted to represent a morphologically inherited ramp system with mesophotic coral mounds developing below the wave base (Fig. 11).

4.2. Taxonomic indicators for mesophotic conditions

The outcrops studied here feature a low coral diversity with ten taxa showing biogeographic affinities to the Arabian Gulf and Mediterranean regions (Pisapia et al., 2024). The dominance of massive poritids, *Favites*, and *Dipsastrea* suggests meso- to oligophotic conditions. The coral frameworks were extensively colonized by encrusting foraminifera, including acervulinids (e.g., *Gypsina*, *Sphaerogypsina*), homotrematids (*Miniacina*), victoriellids (*Biarritzina*), and nubeculariids. Similar assemblages have been reported from Paleocene to Lower Miocene coral mounds and have been interpreted as indicators for oligo-mesophotic conditions (Pomar et al., 2014, 2017). Encrusting biota identified in the Wadi Waqb Member also include melobesioid red algae (*Mesophyllum*, *Sporolithon*), confirming a diminished light availability characterizing the mesophotic realm. Additionally, the inter- and intra-colony matrix contains LBF (relatively flat *Amphistegina*, *Operculina*, *Heterostegina*) that are indicative of mesophotic conditions (cf. Pomar et al., 2017).

While the coral taxa forming the Miocene bioherms show remarkable similarities with modern shallow-water assemblages in the Red Sea (Pisapia et al., 2024), the carbonate facies closely resemble those from modern mesophotic coral ecosystems in the modern Red Sea proper (Westphal et al., 2025). El-Sorogy et al. (2020) interpreted the zooxanthellate corals identified in the Wadi Waqb Member as taxa growing in normal-saline, tropical seas (water temperature of 22–26 °C, minimum 18 °C) in water depths of up to 50 m, rarely reaching 80 m. They also recognized that the corals form isolated build-ups parallel to the shoreline rather than continuous fringing reefs. According to Pisapia et al. (2024), the abundance of massive growth forms including

Poritidae, *Favites*, and *Dipsastraea* points to meso-oligophotic conditions by analogy with ecological assemblages of corals on modern reefs, consistent with the interpretation proposed herein.

4.3. Planktonic and euphotic influence

Along the slope profile, the persistent presence of fragmented and slightly reworked skeletal grains, such as green algae *Halimeda*, articulated red algae *Jania*, and mastophoroids (*Spongites*, *Neogoniolithon*, *Lithoporella*), point to parautochthonous deposition from a shoreward source. Epiphytic foraminifera including symbiont-bearing porcelaneous genera (*Peneroplis*, *Spirolina*, *Dendritina*, *Sivasina*, *Sorites*) further point to phytal substrates such as seagrass beds (e.g., Khokhlova, 2013; Mateu-Vicens et al., 2014). The extinct *Miogypsina globulina* is characterized by lateral chamberlets in both ventral and dorsal sides and, in analogy to the recent genus *Baculogypsinoides,* which hosts symbionts in the lateral chamberlets (Hohenegger, 2011) interpreted to belong to the symbiont-bearing morphotype. *Miogypsina* is known to have thrived in extremely shallow-water environments (e.g., Drooger, 1993; Schiavinotto and Benedetti, 2021), in many cases associated with backreef shoals or seagrass meadows (e.g., Frost et al., 1983; Tournadour et al., 2020). Miogypsinids, in analogy with *Neorotalia* and ornatorotaliids (Benedetti et al., 2025), their possible ancestors, can be considered epiphytic taxa. Sessile and encrusting forms without symbionts, such as *Planorbulina*, are associated with seagrass leaf turnover (Mateu-Vicens et al., 2010), while small miliolids such as *Quinqueloculina* and *Triloculina*, suspension feeders such as *Elphidium*, and facultative motile species with a flat surface of attachment such as cibicidids (*Lobatula*) and rosalinids are common in seagrass and macroalgal habitats (Benedetti and Frezza, 2016; Benedetti et al., 2023). This aligns with a coral mound development in low-energy, meso-oligophotic settings, as observed in the Mediterranean during the Burdigalian (Brandano et al., 2010, 2016) and other Cenozoic systems (Pomar et al., 2014, 2017). The observed ooids in the Wadi Waqb Member support the presence of the very shallow-water carbonate depositional environments fringing the coastline, sedimentologically connected to the deeper, mesophotic, slope depositional environment.

The co-occurrence of planktonic foraminifera with oligophotic-mesophotic biota (e.g., coral frameworks, mesophotic foraminifera) and shallow-water phytal components (e.g., seagrass-associated foraminifera, *Halimeda*) as well as ooids points to a middle- to outer-ramp setting, where sediment accumulation resulted from the combined contribution of shallow-water shedding, autochthonous production, and decantation of the pelagic fraction. Planktonic taxa in the sedimentary matrix include globigerinids (*Globigerinoides ruber*, *G. subquadratus*; *Trilobatus trilobus*, *T. sicanus T. bisphericus*; *Praeorbulina glomerosa*), whose modern analogs thrive in the upper 100 m of the water column (Schiebel and Hemleben, 2017). The absence of deeper-dwelling planktonics further supports deposition in middle to outer ramp settings under open-marine conditions.

The consistent presence of planktonic foraminifera supports deposition in an open-ramp setting, where water exchange was not restricted by barrier reefs isolating a lagoon from the open sea. This interpretation is further supported by the coral growth pattern, which consists of amalgamated mounds distributed along the slope, consistent with mesophotic conditions. Reduced irradiance at these depths likely limited photosynthetic rates and, consequently, carbon assimilation, resulting in lower carbonate accretion rates and explaining the absence of large coral edifices.

In the modern world, mesophotic buildups are typically found in extremely clear, oligotrophic waters at depths greater than 30–50 m (Lesser et al., 2009; Hinderstein et al., 2010; Pyle and Copus, 2019). In case of the deposits studied here, water transparency presumably was low as it was influenced by terrigenous input from the rift graben shoulders, as manifested by the occurrence of quartz and other siliciclastic grains. This detrital contribution suggests that the coral communities may have occupied shallower settings than those typical of the modern mesophotic zone. Nevertheless, the dominance of a fine-grained matrix through most of the succession—except in the uppermost interval at the Al Wajh site—indicates that these ecosystems were generally established below the fair-weather wave base, where background hydrodynamic energy was low. Under such conditions, episodic resuspension events would have increased turbidity and reduced light penetration, making light availability and sediment stress key environmental controls on coral growth and community structure.

4.4. Progradation and productivity

A mesophotic ecology also goes along with the extremely low progradation rates observed for the Wadi Waqb Member. The chronological constraints, based on the occurrence of the planktonic foraminifera *T. bisphericus, T. sicanus*, *Praeorbulina glomerosa* and the benthic species *Miogypsina globulina* (Aquitanian-Burdigalian), place the Wadi Waqb Member precisely in the uppermost Burdigalian (ca. 16.5 Ma), reaching into the Langhian (ca. 14.4 Ma). This age previously had been enigmatic, because age-diagnostic microfossils are scarce and no specific indicators to discriminate Burdigalian from Langhian ages had been reported (see, e.g., Hughes, 2014), and geochemical age dating is not possible because of diagenetic and hydrothermal overprint (own unpublished data). The microbialite drape forming basis of the succession also points to water chemistry deviating from normal marine conditions, presumably influenced by the cul-de-sac position, arid conditions, and thermohaline influence. Presumably the conditions prevailing during the deposition of the basal carbonates of the Wadi Waqb Member were prohibitive towards coral colonization, that only was possible when freshening through the connection to the Mediterranean took place. In this scenario, the microbialites then acted as physical substrate for the coral bioherms as described by Zamagni et al. (2009) for the northern Tethys. Coral growth ended when the Red Sea turned into a saline basin for almost 10 Ma until the end of the Messinian (Segev et al., 2017) and allow to relate the Wadi Waqb Member to other Cenozoic coral buildups, for example from the Mediterranean.

Taking into account that the morphological and stratigraphic top of the coral-dominated carbonate succession has been eroded in the study area, we observe an approximate maximum progradation of less than 1 km in 2 Ma. In contrast to the younger (upper Tortonian) Llucmajor carbonate platform of the Balearic Islands, which prograded at rates an order of magnitude higher (approximately 20 km in 1 Ma; Pomar and Ward, 1995), the progradation rate of the Wadi Waqb Member appears markedly lower, even when accounting for associated uncertainties. This substantial difference suggests significantly reduced carbonate productivity in the Wadi Waqb Member system. The contrast reflects the dominance of a fully developed photozoan carbonate factory in the upper Tortonian Llucmajor platform, whereas carbonate production in the Wadi Waqb Member resulted from a mixed photozoan-heterozoan factory, inherently characterized by lower net accretion rates.

4.5. Comparison with the Mediterranean

From the Cenozoic prior to the Late Miocene, several similar assemblages and architectures of coral-dominated carbonate factories have been described (see extensive review by Pomar et al., 2017). Our interpretation is similar to those of early Cenozoic coral ecosystems from the Mediterranean that are well known to have formed ramp geometries under mesophotic conditions. Most described examples of Cenozoic coral ecosystems in the mesophotic zone are from the Mediterranean Eocene (pre-Pyrenees and Pyrenees, Spain: Plaziat and Perrin, 1992; Eichenseer, 2003; Mateu-Vicens et al., 2012), Oligocene (Apulia, Italy: Bosellini et al., 2021, 2024), and Lower Miocene (Sardinia, Italy, Corsica, France and South-Central Turkey: Bassant et al., 2004; Janson et al., 2007, 2010; Brandano et al., 2016). Pre-upper-Tortonian bioconstructions dominated by small coral buildups with calcareous red

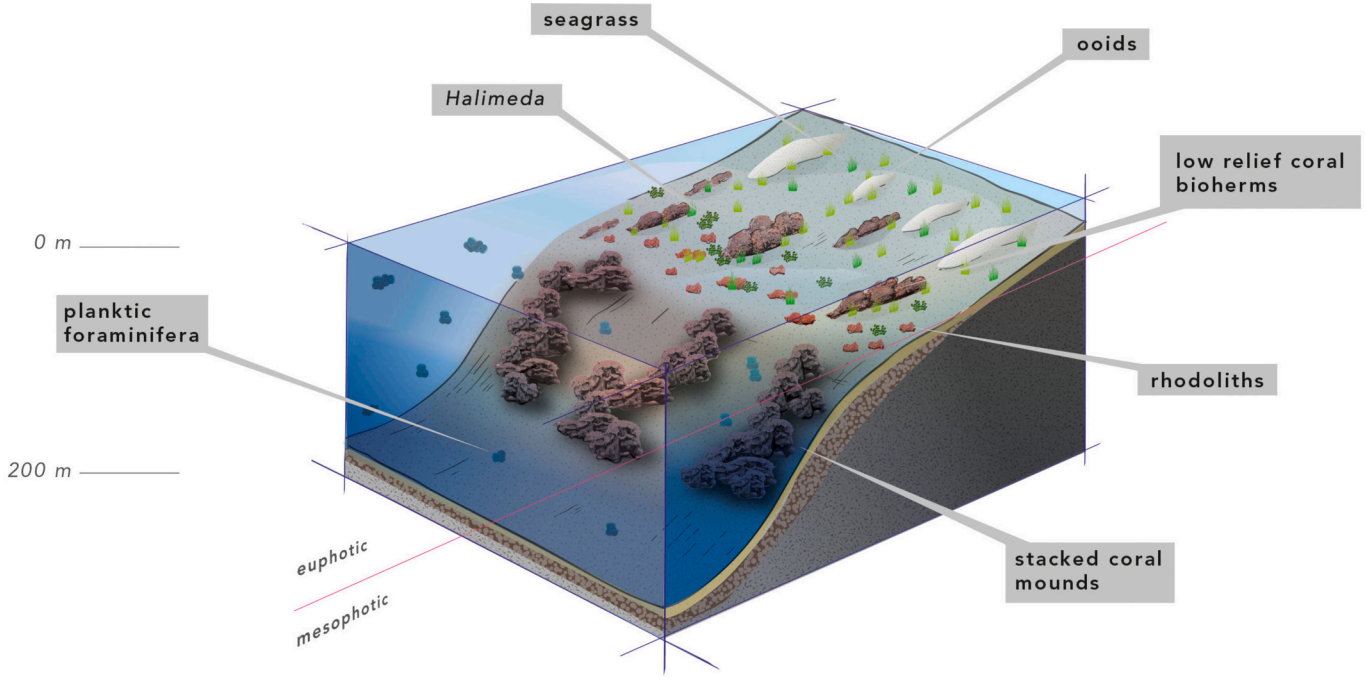

Fig. 12. Depositional model of the carbonate ramp hosting the coral bioherms of the Wadi Waqb Member of the Kibrit Formation (Burdigalian to Langhian, Northern Red Sea, Saudi Arabia). (For interpretation of the references to colour in this figure legend, the reader is referred to the web version of this article.)

algae and encrusting foraminifera were thriving in the mesophotic zone, while the euphotic shallow-water zone was characterized by seagrass meadows (see Pomar and Hallock, 2008; Pomar et al., 2017; Gumati, 1992; Plaziat and Perrin, 1992; Eichenseer, 2003; Spring and Hansen, 1998; Baceta et al., 2005, 2011; Aguirre et al., 2007; Mateu-Vicens et al., 2012; Morsilli et al., 2012). During the Burdigalian, coral development in the Mediterranean occurred primarily within extensional tectonic settings, such as those in Sardinia and Corsica (Casula et al., 2001; Faccenna et al., 2002). These regions were influenced by both tectonic and volcanic activity associated with the opening of the Balearic and Provençal basins, which likely impacted nutrient availability and ocean circulation patterns. Nevertheless, in some aspects the coral bioherms of the Wadi Waqb Member depart significantly from the model established for the Mediterranean pre-late-Tortonian time. For instance, the bioherms studied here exhibit a decreasing relief with shallower water depth along the slope profile, with low-relief structures on the upper slope that are aligned in strike direction (Fig. 6), while the Mediterranean is typically characterized higher-relief bioherms in the upper part of the mesophotic zone (e.g., Brandano et al., 2016).

With the new recalibrated stratigraphy based on the identification of *Miogypsina globulina*, the Wadi Waqb Member can be considered coeval with the Miocene of Corsica (Brandano et al., 2016). In addition to regional tectono-volcanic influences, the late Burdigalian marks the onset of the Monterey Carbon Isotope Excursion, coinciding with the MMCO. These events reflect a period of globally increased seawater fertility and warm, humid conditions (Woodruff and Savin, 1991; Zachos et al., 2001). Given these global and regional changes, including elevated nutrient levels and climatic warming, mesophotic conditions may have provided more favorable settings for coral development. In the case of the Red Sea, characterized by even warmer conditions than the Mediterranean, high surface-water temperatures likely prevented coral colonization in shallow waters, confining coral growth to deeper, cooler mesophotic environments.

4.6. Depositional model

Our interpretation of the overall depositional environment and ecosystem points to a non-actualistic ramp setting with coral mounds, distinctly different to modern shallow-water coral systems which typically feature reef rims and lagoons. Furthermore, the observed presence of in situ coral colonies along the slope profile, in a fine-grained sediment matrix containing euphotic components as well as open water components (*Halimeda* and planktonic foraminifera, respectively), clearly indicate a middle to outer ramp setting, with the coral mounds thriving below the wave base level. The red algal encrustations on the coral colonies and the fine-grained matrix, often including planktonic foraminifera are compatible with open-marine, mesophotic conditions, which is consistent with other coeval examples in the Mediterranean region (Brandano et al., 2016). Our interpretation differs from earlier studies focused on the Wadi Waqb Member in the Midyan area, interpreting the slope sediments as fore-reef of a modern-style coral reef system (e.g., Pensa et al., 2025, 2025b, and references therein). However, modern fore-reef successions are usually devoid of massive in-situ coral bioherms and down-shed *Halimeda* plates which characterize the outcrops studied here. Furthermore, no facies typical for modern coral reef systems, such as lagoonal or reef-crest deposits, were identified in the study area. In fact, the sediments forming the stacked clinoforms show the same general composition throughout, i.e., large *Porites* colonies, fine-grained and poorly sorted matrix, and planktonic foraminifera indicating the open ocean influence. Thus, the geometries are fundamentally different from modern, “Caribbean type”, coral reefs with a euphotic reef rim and a protected lagoon (Pomar et al., 2017). The occurrence of coral taxa in the Wadi Waqb Member that are also present in the euphotic zone of the modern Red Sea (Pisapia et al., 2024) suggests that the evolutionary history of *Symbiodinium* played a role in facilitating the upward migration of corals. This interpretation is consistent with patterns observed in the Miocene Mediterranean (Pomar and Hallock, 2008; Brandano et al., 2016).

The origin of the stratigraphic surfaces that define the clinoforms, and the mechanisms driving progradation in a setting below the wave base, remains unclear. One potential control is syndepositional tectonics, as proposed for deposits in the Midyan region where sediment was remobilized episodically by storms or fault-induced earthquakes (Hughes, 2014). Tectonic activity related to the rifting of the Red Sea

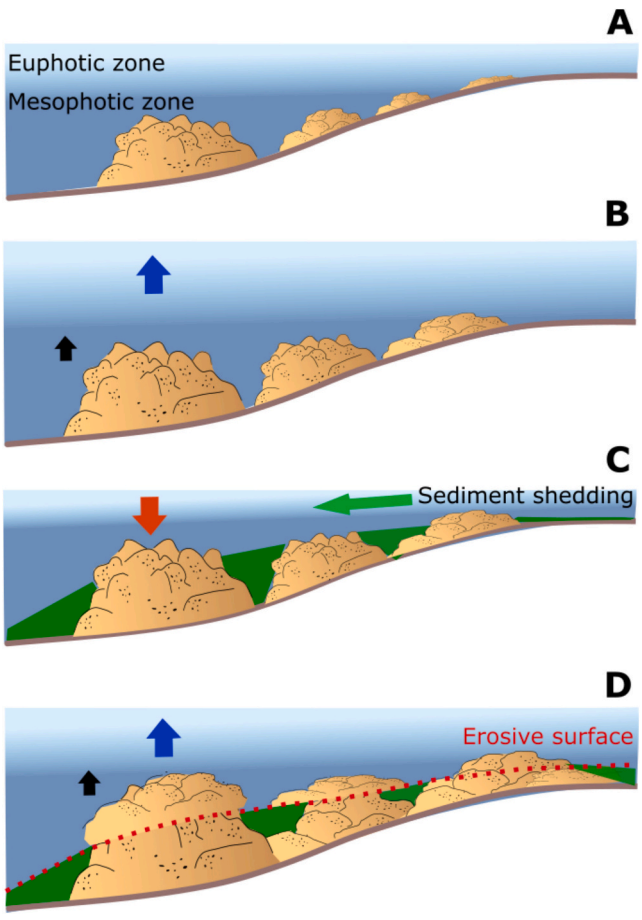

Fig. 13. Ecostratigraphical model of coral mound evolution. Coral growth initiates in the mesophotic zone (A) and continues upward during sea-level rise with limited sediment shedding (B). A sea-level fall increases sediment infill between mounds (C). Renewed sea-level rise fosters new coral growth, forming a new clinoform (D). Red dotted line marks an erosive surface. (For interpretation of the references to colour in this figure legend, the reader is referred to the web version of this article.)

during or shortly after the presence of the coral ecosystems is corroborated by the field evidence for post-depositional hydrothermal fluids locally brecciating and staining the on the carbonate deposits. Alternatively, internal waves generated along a pycnocline may have played a role in shaping the mounded geometries. At the inferred bathymetric range of coral development, a pycnocline may have formed as a result of density gradients driven by continental input and evaporation in a narrow, shallow basin. Under these conditions, internal waves propagating along the pycnocline could have enhanced nutrient transport towards the coral ecosystems (Pomar et al., 2017). The buildups could also have been bathymetrically constrained by light availability, as suggested for coeval similar systems in Corsica (Brandano et al., 2016; Tomassetti et al., 2013). Similar as described from the Midyan region (Hughes, 2014), the outcrops of the Wadi Waqb Member in the Al Wajh and Umluj areas are discontinuous, and their relatively poor preservation hinders the identification of erosion surfaces and other discontinuities in the geological record.

Considering the ecological significance of the identified components, which enable estimation of the bathymetric position within the system, and applying an ecostratigraphic approach (sensu Pomar, 2020), a depositional model is proposed (Fig. 12) in which coral buildup initiated within the mesophotic zone. This development occurred during a phase of global climatic reorganization associated with the MMCO, followed by the Miocene Climatic Transition at the onset of the Middle Miocene (Miller et al., 2020), corresponding to the age of the Wadi Waqb Member. The sea-level fluctuations linked to this climatic variability likely operated at multiple scales, with higher-frequency, lower-amplitude cycles superimposed on longer-term trends, exerting strong control on carbonate accretion patterns (Fig. 13). During transgressive phases, corals would have attempted to maintain their position within the photic zone through vertical aggradation, leading to mound formation. Corals established at greater depths would have required higher growth rates to remain within the lighted zone, which may explain why some buildups are larger and more elevated than others along the slope. Bioclastic sediment shedding during this initial phase would have been very limited. Subsequently, during a high-frequency relative sea-level fall, sediment shedding increased, promoting the accumulation of sediment between coral mounds. This process likely smoothed the slope and led to interfingering between sediments and coral bioconstructions. With the ensuing sea-level rise, the underlying coral mounds and interfingered sediments provided a suitable substrate for the development of new coral bioconstructions, which initiated the formation of a new clinoform.

5. Conclusions

The present study is the first ecological interpretation of the Miocene Wadi Waqb Member (Saudi Arabia) at the southern reaches of its occurrence, and thus at the southern extension of the marine flooding of the incipient Red Sea at that time. The Wadi Waqb Member is of late Burdigalian to Langhian age, as indicated by the LBF *Miogypsina globulina* at the base of the succession, which, together with planktonic foraminifera assemblages, is in agreement with previous studies (N7–N8). Carbonates of the Wadi Waqb Member were deposited on a ramp predefined by erosional morphology. Large coral colony stacks formed in the mesophotic environments on the slope of the ramp, with smaller colonies developed on the upper ramp where the carbonate depositional system grades towards euphotic conditions. The presence of ooid shoals and seagrass meadows in adjacent euphotic settings is evidenced by allochthonous ooids and epiphytic foraminifera preserved in the slope sediments. The non-actualistic depositional model for the Wadi Waqb Member proposed here is similar to coeval and older Cenozoic coral ecosystems from the Mediterranean, interpreted as mesophotic, environments with a non-stratified water column (cf. Pomar et al., 2017). Our study thus corroborates the hypothesis that modern coral reefs developed only after the late Cenozoic cooling, migrating into shallower environments after water-column stratification developed.

CRediT authorship contribution statement

Guillem Mateu Vicens: Writing – review & editing, Writing – original draft, Methodology, Investigation, Formal analysis, Conceptualization. **Marco Brandano:** Writing – review & editing, Writing – original draft, Validation, Investigation, Formal analysis, Conceptualisation. **Patrick Boyden:** Writing – review & editing, Writing – original draft, Visualization, Software, Methodology, Investigation, Formal analysis. **Andrea Benedetti:** Writing – review & editing, Writing – original draft, Investigation, Formal analysis. **Jan-Peter Duda:** Writing – review & editing, Writing – original draft, Investigation, Formal analysis. **Hildegard Westphal:** Writing – review & editing, Writing – original draft, Validation, Supervision, Resources, Project administration, Methodology, Investigation, Funding acquisition, Formal analysis, Data curation, Conceptualization.

Declaration of competing interest

All authors declare no conflict of interest.

Acknowledgements

We acknowledge the reviews by Ben Rendall and an anonymous reviewer that helped to improve the manuscript. The authors are grateful to Red Sea Global for access to the study area, and to Alexander Petrovic, Thomas Teillet, Tihana Pensa, Chiara Pisapia, and Nicolas Boehm (all KAUST), Marlena Joppien and Lea Tabea Fuchs (University of Bremen/KAUST), and Eike C. Bornholdt (University of Potsdam) for their help in the field. We thank Aboud al Afifi and Volker Vahrenkamp (KAUST) for useful information for preparing the field work. The drone survey was undertaken by FalconViz (Thuwal, Saudi Arabia); thanks are due to Khaled Abdelgawad and his team for this collaboration. This study is part of a larger project on the Miocene deposits of the northern Saudi Arabian Red Sea coast and was funded through King Abdullah University of Science and Technology (KAUST) baseline funding to Hildegard Westphal. Guillem Mateu Vicens has been funded by the Ministerio de Ciencia e Innovación of the Spanish Government (project PID2022-137860NB-I00).

Appendix A. Supplementary data

Supplementary data to this article can be found online at https://doi.org/10.1016/j.palaeo.2026.113874.

Data availability

The authors confirm that all data necessary for supporting the scientific findings of this paper have been provided.

References

Aguirre, J., Baceta, J.I., Braga, J.C., 2007. Recovery of marine primary producers after the cretaceous Tertiary mass extinction: paleocene calcareous red algae from the Iberian Peninsula. Palaeogeogr. Palaeoclimatol. Palaeoecol. 249, 393–411.

Al-Kahtany, K.M., 2017. Facies development of the Middle Miocene reefal limestone in Northwest Saudi Arabia. J. Afr. Earth Sci. 130, 134–140. https://doi.org/10.1016/j.jafrearsci.2017.03.012.

Augustin, N., van der Zwan, F.M., Devey, C.W., Brandsdóttir, B., 2021. 13 million years of seafloor spreading throughout the Red Sea Basin. Nat. Commun. 12 (1), 2427.

Baceta, J.I., Pujalte, V., Bernaola, G., 2005. Paleocene coralgal reefs of the western Pyrenean basin, northern Spain: new evidence supporting an earliest Paleogene recovery of reefal ecosystems. Palaeogeogr. Palaeoclimatol. Palaeoecol. 224, 117–143.

Baceta, J.I., Pujalte, V., Wright, V.P., Schmitz, B., 2011. Carbonate platform models, sea-level changes and extreme climatic events during the Paleocene-early Eocene greenhouse interval: a basin-platform-coastal plain transect across the southern Pyrenean basin. In: Arenas, C., Pomar, L., Colombo, F. (Eds.), Pre- Meeting Field Trips Guidebook, 28th IAS Meeting, vol. 7. Sociedad Geológica de España, Geo-Guías, Zaragoza, pp. 151–198.

Bassant, P., Van Buchem, F.S.P., Strasser, A., Lomando, T., 2004. A comparison of two early Miocene carbonate margins: the Zhujiang carbonate platform (subsurface, South China) and the Pirinç platform (outcrop, Southern Turkey). In: Grammer, M., Harris, P.M. (Eds.), Integration of Outcrop and Modern Analogs in Reservoir Modeling, vol. 80, pp. 153–170. AAPG Mem.

Bassi, D., Braga, J.C., Di Domenico, G., Pignatti, J., Abramovich, S., Hallock, P., Könen, J., Kovács, Z., Langer, M.R., Pavia, G., Iryu, Y., 2021. Palaeobiogeography and evolutionary patterns of the larger foraminifer *Borelis* de Montfort (Borelidae). Pap. Palaeontol. 7, 377–403.

Bassi, D., Braga, J.C., Pignatti, J., Fujita, K., Nebelsick, J.H., Renema, W., Iryu, Y., 2024. Porcelaneous larger foraminiferal responses to Oligocene–Miocene global changes. Palaeogeogr. Palaeoclimatol. Palaeoecol. 634, 111916. https://doi.org/10.1016/j.palaeo.2023.111916.

Benedetti, A., Frezza, V., 2016. Benthic foraminiferal assemblages from shallow-water environments of northeastern Sardinia (Italy, Mediterranean Sea). Facies 62, 14.

Benedetti, A., Gaglianone, G., Brandano, M., Mateu-Vicens, G., 2023. Recent benthic foraminiferal assemblages and sedimentary facies from two atolls of Maldivian Archipelago (Indian Ocean): reef and seagrass indicators. Mar. Geol. 464, 107143. https://doi.org/10.1016/j.margeo.2023.107143.

Benedetti, A., Briguglio, A., Consorti, L., Papazzoni, C.A., 2025. Paleoecological and paleoenvironmental insights from Ornatorotaliidae (larger foraminifera). Mar. Micropaleontol. 194, 102423. https://doi.org/10.1016/j.marmicro.2024.102423.

Bosellini, A., 1984. Progradation geometries of carbonate platforms: examples from the Triassic of the Dolomites, northern Italy. Sedimentology 31, 1–24.

Bosellini, F.R., Vescogni, A., Budd, A.F., Papazzoni, C.A., 2021. High coral diversity is coupled with reef-building capacity during the late Oligocene warming (Castro limestone, Salento Peninsula, S. Italy). Riv. Ital. Paleontol. Stratigr. 127 (3), 515–538. https://doi.org/10.13130/2039-4942/16332.

Bosellini, F.R., Vescogni, A., Briguglio, A., Piazza, M., Papazzoni, C.A., Silvestri, G., Morsilli, M., 2024. Resilient coral reef ecosystems: the case study of turbid-mesophotic coral buildups during the late Oligocene Warming Event (Tertiary Piedmont Basin, NW Italy). Palaeogeogr. Palaeoclimatol. Palaeoecol. 649, 112330. https://doi.org/10.1016/j.palaeo.2024.112330.

Bosellini, F.R., Benedetti, A., Kiessling, W., 2025. Minor coral diversity loss but long-lasting coral reef crises in the early Paleogene hothouse. Paleoceanogr. Paleoclimatol. 40, e2024PA004985. https://doi.org/10.1029/2024PA004985.

Bosworth, W., Huchon, P., McClay, K., 2005. The Red Sea and Gulf of Aden basins. J. Afr. Earth Sci. 43, 334–378.

Bosworth, W., Khalil, S.M., Ligi, M., Stockli, D.F., McClay, K.R., 2020. Geology of Egypt: the Northern Red Sea. In: Geol. Egypt, pp. 343–374.

BouDagher-Fadel, M.K., 2015. Biostratigraphic and Geological Significance of Planktonic Foraminifera. UCL Press, London, p. 306. https://doi.org/10.2307/j.ctt1g69xwk.

BouDagher-Fadel, M., Price, G., 2013. The phylogenetic and palaeogeographic evolution of the miogypsinid larger benthic foraminifera. J. Geol. Soc. Lond. 170, 185–208. https://doi.org/10.1144/jgs2011-149.

Brandano, M., Tomassetti, L., Bosellini, F., Mazzucchi, A., 2010. Depositional model and paleodepth reconstruction of a coral-rich, mixed siliciclastic-carbonate system: the Burdigalian of Capo Testa (northern Sardinia, Italy). Facies 56, 433–444.

Brandano, M., Bosellini, F.R., Mazzucchi, A., Tomassetti, L., 2016. Coral assemblages and biocostructions adapted to the depositional dynamics of a mixed carbonate-siliciclastic setting: the case study of the Burdigalian Bonifacio Basin (South Corsica). Rivist. Paleontol. Stratigr. Ital. 122, 37–52.

Brandano, M., Tomassetti, L., Cornacchia, I., 2019. The lower Rupelian cluster reefs of Majella platform, the shallow water record of Eocene to Oligocene transition. Sedimentary Geology 380, 21–30. https://doi.org/10.1016/j.sedgeo.2018.11.013.

Briguglio, A., 2018. The Miocene (Burdigalian) lepidocyclinids and miogypsinids of Channa Kodi, Padappakkara, Southern India. Palaeontogr. A Palaeozool. Stratigr. 312 (1–4), 1–15.

Buxton, M., Pedley, H.M., 1989. A standardised model for Tethyan Tertiary carbonate ramps. J. Geol. Soc. 146, 746–748. https://doi.org/10.1144/gsjgs.146.5.0746.

Camp, V.E., Roobol, M.J., 1992. Upwelling asthenosphere beneath western Arabia and its regional implications. J. Geophys. Res. 97 (B11), 15255–15271.

Casula, G., Cherchi, A., Montadert, L., Murru, M., Sarria, E., 2001. The Cenozoic graben system of Sardinia (Italy): geodynamic evolution from new seismic and field data. Mar. Pet. Geol. 18 (7), 863–888.

DeCarlo, T.M., Karnauskas, K.B., Davis, K.A., Wong, G.T.F., 2015. Climate modulates internal wave activity in the Northern South China Sea. Geophys. Res. Lett. 42, 831e838. https://doi.org/10.1002/2014GL062522.

Degen, T., Sadki, M., Bron, E., König, U., Nénert, G., 2014. The HighScore suite. Powder Diffract. 29 (S2), S13–S18. https://doi.org/10.1017/S0885715614000840.

Drooger, C.W., 1993. Radial Foraminifera; morphometrics and evolution. Verh Koninkl. Nederl. Akad. Wetensch Afd. Natuurk. 41, 1–242.

Dunham, R.J., 1962. Classification of carbonate rocks according to depositional texture. In: Ham, W.E. (Ed.), Classification of Carbonate Rocks: AAPG Memoir, 1, pp. 108–121.

Eichenseer, H., 2003. Stratigraphic styles influenced by thrust tectonics: Architecture and facies of lowstand wdges and transgressive to highstand carbonate banks (upper Paleocene to lower Eocene, Central-Southern Pyrenees). Geological Field Trip 4. In: AAPG International Conference and Exhibition 2003, Barcelona, Spain, p. 77.

El-Sorogy, A.S., Tsaparas, N., Al-Kahtany, K., 2020. Middle Miocene corals from Midyan area, Northwestern Saudi Arabia. Geol. J. 1–12. https://doi.org/10.1002/gj.3761.

Faccenna, C., Speranza, F., Caracciolo, F.D.A., Mattei, M., Oggiano, G., 2002. Extensional tectonics on Sardinia (Italy): insights into the arc–back-arc transitional regime. Tectonophysics 356 (4), 213–232.

Frost, S.H., Harbour, J.L., Beach, D.K., Realini, M.J., Harris, P.M., 1983. Oligocene reef tract development, southwestern Puerto Rico. Sedimenta 9, 132.

Gumati, Y.D., 1992. Lithostratigraphy of oil-bearing Tertiary bioherms in the Sirte basin, Libya. J. Pet. Geol. 15, 305–318.

Hardy, R.G., Tucker, M., 1988. X-ray powder diffraction of sediments. In: Tucker, M. (Ed.), Techniques in Sedimentology. Blackwell, Oxford, pp. 191–228.

Hinderstein, L.M., Marr, J.C.A., Martinez, F.A., Dowgiallo, M.J., Puglise, K.A., Pyle, R.L., Zawada, D.G., et al., 2010. Theme section on "Mesophotic Coral Ecosystems: characterization, Ecology, and Management". Coral Reefs 29, 247–251.

Hohenegger, J., 2011. Large Foraminifera: Greenhouse Constructions and Gardeners in the Oceanic Microcosm. Kagoshima University Museum, Kagoshima, p. 81.

Hughes, G.W., 2014. Micropalaeontology and palaeoenvironments of the Miocene Wadi Waqb carbonate of the northern Saudi Arabian Red Sea. GeoArabia 19 (4), 59–108. https://doi.org/10.2113/geoarabia190459.

Hughes, G.W., Johnson, R.S., 2005. Lithostratigraphy of the Red Sea. GeoArabia 10 (3), 49–126.

Hussain, M., Al-Ramadan, K., 2009. Microfacies analysis of Wadi Waqb Member (Miocene) in Wadi Aynunah, northwest of Saudi Arabia. Carbonates Evaporites 24, 139–149.

Insalaco, E., 1998. The descriptive nomenclature and classification of growth fabrics in fossil scleractinian reefs. Sediment. Geol. 118, 159–186.

Janson, X., Eberli, G., Bonnaffe, F., Gaumet, F., De Casanove, V., 2007. Seismic expression of a Miocene prograding carbonate margin, Mut Basin, Turkey. AAPG Bull. 91, 685–713.

Janson, X., Van Buchem, F.S.P., Dromart, G., Eichenseer, H.T., Dellamonica, X., Boichard, R., Bonnaffe, F., Eberli, G., 2010. Architecture and facies differentiation within a middle Miocene carbonate platform, Ermenek, Mut basin, southern Turkey. In: Van Buchem, F.S.P., Gerdes, K.D., Esteban, M. (Eds.), Mesozoic and Cenozoic Carbonate Systems of the Mediterranean and the Middle East: Stratigraphic and Diagenetic Reference Models. Geol. Soc., London, pp. 265–290. Spec. Publ.

Jones, R.W., Simmons, M.D., Whittaker, J.E., 2006. On the stratigraphical and palaeobiogeographical significance of *Borelis melo melo* (Fichtel & Moll, 1978) and *B. melo curdica* (Reichel, 1937) (Foraminifera, Miliolida, Alveolinidae). Journal of Micropalaeontology 25 (2), 175–185.
Khokhlova, A., 2013. Epiphytic foraminiferal indices as bioidicators in Mediterranean seagrass meadows: Unpublished Master Dissertation, Universitat de les Illes. Balears 38.
Lesser, M.P., Slattery, M., Leichter, J.J., 2009. Ecology of mesophotic coral reefs. J. Exp. Mar. Biol. Ecol. 375 (1–2), 1–8.
Loeblich, A.R., Tappan, H., 1987. Foraminiferal Genera and Their Classification: Volume I and II. Van Nostrand Reinhold, New York.
Martín-Martín, M., Miclăuș, C., Tent-Manclús, J.E., Tosquella, J., Serrano, F., Samsó, J. M., Martín-Pérez, J.A., 2025. Paleocene-Eocene evolution of the Prebetics (South Iberian Margin, South Spain) and comparison with other western Tethyan margins. Marine and Petroleum Geology 176, 107300. https://doi.org/10.1016/j.marpetgeo.2025.107300.
Mateu-Vicens, G., Box, A., Deudero, S., Rodriguez, B., 2010. Comparative analysis of epiphytic foraminifera in sediments colonized by seagrass *Posidonia oceanica* and invasive macroalgae *Caulerpa* spp. J. Foraminifer. Res. 40, 134–147.
Mateu-Vicens, G., Pomar, L., Ferrandez-Cañadell, C., 2012. Nummulitic banks in the upper Lutetian "Buil level", Ainsa basin, south Central pyrenean zone: the impact of internal waves. Sedimentology 59, 527–552. https://doi.org/10.1111/j.1365-3091.2011.01263.x.
Mateu-Vicens, G., Khokhlova, A., Sebastián-Pastor, T., 2014. Epiphytic foraminiferal indices as bioindicators in Mediterranean seagrass meadows. J. Foraminifer. Res. 44 (3), 325–339. https://doi.org/10.2113/gsjfr.44.3.325.
McClay, K.R., G.J. Nichols, S. Khalil, M. Darwish, W. Bosworth (1998) Extensional tectonics and sedimentation, eastern Gulf of Suez, Egypt. In: Purser, B.H. and D.W.J. Bosence (eds.) Sedimentation and Tectonics in Rift Basins. Red Sea – Gulf of Aden. Chapman & Hall, pp. 223–238.
Miller, K.G., Browning, J.V., Schmelz, W.J., Kopp, R.E., Mountain, G.S., Wright, J.D., 2020. Cenozoic sea-level and cryospheric evolution from deep-sea geochemical and continental margin records. Sci. Adv. 6 (20), eaaz1346.
Montaggioni, L.F., Braithwaite, C.J., 2009. Quaternary Coral Reef Systems: History, Development Processes and Controlling Factors. Elsevier, Amsterdam, p. 550.
Morsilli, M., Bosellini, F.R., Pomar, L., Hallock, P., Papazzoni, C.A., Aurell, M., 2012. Mesophotic coral buildups in a prodelta setting (late Eocene, southern Pyrenees, Spain): a mixed carbonate siliciclastic system. Sedimentology 59, 766–794. https://doi.org/10.1111/j.1365-3091.2011.01275.x.
Öğretmen, N., Giovenzana, F., Khalifa, A., Mateu-Vicens, G., Westphal, H., 2025. The extreme Red Sea and its late Cenozoic shallow water benthic foraminifers. Disc. Oceans 2, 35. https://doi.org/10.1007/s44289-025-00073-6.
Orszag-Sperber, F., Harwood, G., Kendall, A., Purser, B.H. (1998) A review of the evaporites of the Red Sea-Gulf of Suez rift. In: Purser, B.H., Bosence D.W.J. (Eds.), Sedimentation and Tectonics of Rift Basins: Red Sea-Gulf of Aden, Chapman & Hall, London (1998), pp. 409–426, https://doi.org/10.1007/978-94-011-4930-3_22.
Patruno, S., Helland-Hansen, W., 2018. Clinoforms and clinoform systems: review and dynamic classification scheme for shorelines, subaqueous deltas, shelf edges and continental margins. Earth Sci. Rev. 185, 202–233. https://doi.org/10.1016/j.earscirev.2018.05.016.
Pensa, T., Baby, G., Teillet, T., et al., 2025. Evolution of carbonate platforms in the Northeast Red Sea during the last 23 million years. Sci. Rep. 15, 10332. https://doi.org/10.1038/s41598-025-92219-x.
Pensa, T., Baby, G., Teillet, T., Delaunay, A., Afifi, A., 2025b. Geometry of Middle Miocene Carbonates in the Red Sea: Outcrop Analogues for Fault-Block Carbonate Platforms in Rift Basins. Paper presented at the Middle East Oil, Gas and Geosciences Show (MEOS GEO), Manama, Bahrain, September 2025. https://doi.org/10.2118/227262-MS.
Perrin, C., 2002. Tertiary: the emergence of modern reef ecosystems. In: Flügel, E., Kiessling, W., Golonka, J. (Eds.), Phanerozoic Reef Patterns: SEPM Special Publication 72, pp. 587–618.
Perrin, C., Plaziat, J.-C., Rosen, B.R., 1998. Miocene coral reefs and reef corals of the South-Western Gulf of Suez and North-Western Red Sea distribution, diversity, and regional environmental control. In: Purser, B.H., Bosence, D.W.J. (Eds.), Sedimentation and Tectonics in Rift Basins. Red Sea – Gulf of Aden. Chapman & Hall, pp. 296–320.
Pisapia, C., Mateu Vicens, G., Benzoni, F., Westphal, H., 2024. Mediterranean imprint on coral diversity in the incipient Red Sea (Burdigalian, Saudi Arabia). Palaios 39, 233–242. https://doi.org/10.2110/palo.2023.025.
Plaziat, J.C., Perrin, C., 1992. Multikilometer-sized reefs built by foraminifera (*Solenomeris*) from the early Eocene of the Pyrenean domain (S. France, N. Spain): paleoecologic relations with coral reefs. Palaeogeogr. Palaeoclimatol. Palaeoecol. 96, 195–231.
Pochon, X., Montoya-Burgos, J.I., Stadelmann, B., Pawlowski, J., 2006. Molecular phylogeny, evolutionary rates, and divergence timing of the symbiotic dinoflagellate genus Symbiodinium. Mol. Phylogenet. Evol. 38, 20–30.
Pomar, L., 2020. Carbonate systems (Chapter 12). In: Scarselli, N., Adam, J., Chiarella, D., Roberts, D.G., Bally, A.W. (Eds.), Regional Geology and Tectonics (Second Edition). Elsevier, pp. 235–311.
Pomar, L., Hallock, P., 2007. Changes in coral-reef structure through the Miocene in the Mediterranean province: adaptive versus environmental influence. Geology 35, 899–902. https://doi.org/10.1130/G24034A.1.
Pomar, L., Hallock, P., 2008. Carbonate factories: a conundrum in sedimentary geology. Earth Sci. Rev. 87, 134–169. https://doi.org/10.1016/j.earscirev.2007.12.002.
Pomar, L., Ward, W.C., 1995. Sea-level changes, carbonate production and platform architecture: the Llucmajor Platform, Mallorca, Spain. In: Haq, B. (Ed.), Sequence Stratigraphy and Depositional Response to Eustatic, Tectonic and Climatic Forcing. Kluwer Academic, Dordrecht, pp. 87–112.
Pomar, L., Mateu-Vicens, G., Morsilli, M., Brandano, M., 2014. Carbonate ramp evolution during the late Oligocene (Chattian), Salento Peninsula, southern Italy. Palaeogeogr. Palaeoclimatol. Palaeoecol. 404, 109–132. https://doi.org/10.1016/j.palaeo.2014.03.023.
Pomar, L., Baceta, J.I., Hallock, P., Mateu-Vicens, G., Basso, D., 2017. Reef building and carbonate production modes in the west-central Tethys during the Cenozoic. Mar. Pet. Geol. 83, 261–304.
Pyle, R.L., Copus, J.M., 2019. Mesophotic coral ecosystems: introduction and overview. In: Loya, Y., Puglise, K.A., Bridge, T.C.L. (Eds.), Mesophotic Coral Ecosystems. Springer, New York, NY, USA, pp. 3–27.
Quiquerez, A., Dromart, G., 2006. Environmental control on granular clinoforms of ancient carbonate shelves. Geol. Mag. 143 (3), 343–365.
Rasul, N.M.A., Stewart, I.C.F., Nawab, Z.A., 2015. Introduction to the Red Sea: its origin, structure, and environment. In: Rasul, N.M.A., Stewart, I.C.F., Nawab, Z.A. (Eds.), The Red Sea – The Formation, Morphology, Oceanography and Environment of a Young Ocean Basin. Springer, Heidelberg, pp. 1–28.
Roozpeykar, A., Moghaddam, I.M., Yaazdi, M., Yousefi, B., 2021. Burdigalian-Langhian foraminifera of the northwest High Zagros Thrust Belt, southwest Iran. Geologos 27 (2), 115–126.
Scardino, G., Rovere, A., Barile, C., Nandasena, N.A.K., Chauveau, D., Dahm, M., Boyden, P., Bejarano, S., Casella, E., Kelly, H., Mijts, E., Scicchitano, G., 2025. Coastal boulders emplaced by extreme wave events impacting the ABC islands (Aruba, Bonaire, Curaçao; Leeward Antilles, Caribbean). Quat. Sci. Rev. 349, 109136. https://doi.org/10.1016/j.quascirev.2024.109136.
Schiavinotto, F., Benedetti, A., 2021. *Nephrolepidina* and unispiralled Miogypsinidae from the Oligo-Miocene toe-of-slope succession of Gran Sasso (L'aquila, Central Apennines - Italy): biometric and evolutionary remarks. Micropaleontology 67, 483–514.
Schiebel, R., Hemleben, C., 2017. Planktic Foraminifers in the Modern Ocean. Springer-Verlag, Berlin.
Segev, A., Avni, Y., Shahar, J., Wald, R., 2017. Late Oligocene and Miocene different seaways to the Red Sea–Gulf of Suez rift and the Gulf of Aqaba–Dead Sea basins. Earth-Sci. Rev. 171, 196–219. https://doi.org/10.1016/j.earscirev.2017.05.004.
Serra-Kiel, J., Gallardo-Garcia, A., Razin, P.H., Robinet, J., Roger, J., Grelaud, C., Leroy, S., Robin, C., 2016. Middle Eocene-Early Miocene larger foraminifera from Dhofar (Oman) and Socotra Island (Yemen). Arabian Journal of Geosciences 9 (3), 1–95.
Sirel, E., Özgen-Erdem, N., Kangal, Ö., 2013. Systematics and biostratigraphy of Oligocene (Rupelian-Early Chattian) foraminifera from lagoonal-very shallow water limestone in the eastern Sivas Basin (central Turkey). Geologia Croatica 66 (2), 83–109.
Spring, D., Hansen, O., 1998. The influence of platform morphology and sea level on the development of a carbonate sequence: the Harash Formation, Eastern Sirt Basin. Libya Geol. Soc. Lond. Spec. Publ. 132, 335–353. https://doi.org/10.1144/GSL.SP.1998.132.01.19.
Stephen, R.P., Michael, T.A., Charles, R.B., William, B.M., David, J.R., David, M.S., Andrei, T., Mark, V.W., 2005. Preferential deposition and preservation of structurally-controlled synrift reservoirs: Northeast Red Sea and Gulf of Suez. GeoArabia 10, 97–124.
Stern, R.J., Johnson, P.R., 2019. Constraining the opening of the Red Sea: evidence from the Neoproterozoic margins and Cenozoic magmatism for a volcanic rifted margin. In: Rasul, N.M.A., Stewart, I.C.F. (Eds.), Geological Setting, Palaeo-Environment and Archaeology of the Red Sea. Springer, Switzerland, pp. 53–81.
Tomassetti, L., Bosellini, F.R., Brandano, M., 2013. Growth and demise of a Burdigalian coral bioconstruction on a granite rocky substrate (Bonifacio Basin, southeastern Corsica). Facies 59, 703–716.
Torfstein, A., Steinberg, J., 2020. The Oligo–Miocene closure of the Tethys Ocean and evolution of the proto-Mediterranean Sea. Sci. Rep. 10, 1–10.
Tournadour, E., Fournier, F., Etienne, S., Collot, J., Maurizot, P., Patriat, M., Sevin, B., Morgans, H.E.G., Martin-Garin, B., Braga, J.C., 2020. Seagrass-related carbonate ramp development at the front of a fan delta (Burdigalian, New Caledonia): insights into mixed carbonate-siliciclastic environments. Mar. Pet. Geol. 121, 104581. https://doi.org/10.1016/j.marpetgeo.2020.104581.
Tubbs, R.E., Fouda, H.G.A., Afifi, A.N., Raterman, N.S., Hughes, G.W., Fadolalkarem, Y. K., 2014. Midyan Peninsula, northern Red Sea, Saudi Arabia: seismic imaging and regional interpretation. GeoArabia 19 (3), 165–184.
Tusberti, F., Chimento, F., Brandano, M., Breda, A., Massironi, M., Perissinotto, M.L., Tomassetti, L., Preto, N., 2024. Geometry and stratigraphic relationships of lower Oligocene coral reefs in Lumignano (Berici Hills, northern Italy). Ital. J. Geosci. 143, 25–36. https://doi.org/10.3301/IJG.2024.02.
Vecsei, A., Sanders, D.G., 1997. Sea-level highstand and lowstand shedding related to shelf margin aggradation and emersion, Upper Eocene-Oligocene of Maiella carbonate platform, Italy. Sedimentary Geology 112 (3–4), 219–234.
Vogt, C., Lauterjung, J., Fischer, R.X., 2002. Investigation of the clay fraction (<2 μm) of the clay mineral society reference clays. Clay Clay Miner. 50 (3), 388–400.
Wade, B.S., Pearson, P.N., Berggren, W.A., Pälike, H., 2011. Review and revision of Cenozoic tropical planktonic foraminiferal biostratigraphy and calibration to the geomagnetic polarity and astronomical time scale. Earth Sci. Rev. 104, 111–142.
Westphal, H., Marchese, F., Giovenzana, F., Mateu Vicens, G., Brandano, M., Bracchi, V. A., Vimercati, S., Vahrenkamp, V., Kanamatsu, T., Petrovic, A., 2025. Depth diagnostic mesophotic assemblages in the Northern Red Sea (Saudi Arabia) as analogue to the Cenozoic fossil record. Coral Reefs. https://doi.org/10.1007/s00338-025-02630-z.

Woodruff, F., Savin, S., 1991. Mid-Miocene isotope stratigraphy in the deep sea: high-resolution correlations, paleoclimatic cycles, and sediment preservation. Paleoceanography 6 (6), 755–806.
Yazdi-Moghadam, M., Sadeghi, A., Adabi, M.H., Tahmasbi, A., 2018. Foraminiferal biostratigraphy of the lower Miocene Hamzian and Arashtanab sections (NW Iran), northern margin of the Tethyan Seaway. Geobios 51, 231–246.
Zachos, J., Pagani, M., Sloan, L., Thomas, E., Billups, K., 2001. Trends, rhythms, and aberrations in global climate 65 Ma to present. Science 292, 686–693.
Zamagni, J., Košir, A., Mutti, M., 2009. The first microbialite—coral mounds in the Cenozoic (Uppermost Paleocene) from the Northern Tethys (Slovenia): environmentally triggered phase shifts preceding the PETM? Palaeogeogr. Palaeoclimatol. Palaeoecol. 274, 1–17.